Synthesis and Characterization of Ru(II) Tris(1,10-phenanthroline)-Electron Acceptor Dyads Incorporating the 4-Benzoyl-*N*-methylpyridinium Cation or *N*-Benzyl-*N*′-methyl Viologen. Improving the Dynamic Range, Sensitivity, and Response Time of Sol−Gel-Based Optical Oxygen Sensors

Nicholas Leventis,*,† Abdel-Monem M. Rawashdeh,‡ Ian A. Elder,‡ Jinhua Yang,‡ Amala Dass,‡ and Chariklia Sotiriou-Leventis*,‡

NASA Glenn Research Center, Materials Division/Polymers Branch, 21000 Brookpark Road, M.S. 49-1, Cleveland, Ohio 44135, and Department of Chemistry, University of Missouri−Rolla, Rolla, Missouri 65409

Received October 13, 2003. Revised Manuscript Received February 11, 2004

The title compounds were synthesized by Sonogashira coupling reactions of appropriate Ru(II) complexes with the electron acceptors. Characterization was conducted in solution and in frozen matrixes. Finally, the title compounds were evaluated as dopants of sol−gel materials. It was found that the intramolecular quenching efficiency of 4-benzoyl-*N*-methylpyridinium cation in solution depends on the solvent: photoluminescence is quenched completely in CH_3CN, but not in methanol or ethanol. On the other hand, intramolecular emission quenching by 4-benzyl-*N*-methyl viologen is complete in all solvents. The difference between the two quenchers is traced electrochemically to the solvation of the 4-benzoyl-*N*-methylpyridiniums by alcohol. In frozen matrixes or adsorbed on the surfaces of silica aerogel, both Ru(II) complex/electron acceptor dyads of this study are photoluminescent, and the absence of quenching has been traced to the environmental rigidity. When doped aerogels are cooled at 77 K, the emission intensity increases by ∼4×, and the spectra shift to the blue, analogous to what is observed with Ru(II) complexes in solutions undergoing fluid-to-rigid transition. However, in contrast to frozen solutions, the luminescent moieties in the bulk of aerogels kept at low temperatures are still accessible to gas-phase quenchers diffusing through the mesopores, leading to more sensitive platforms for sensors than other room-temperature configurations. Thus, the photoluminescence of our Ru(II) complex dyads adsorbed on aerogel is quenchable by O_2 both at room temperature and at 77 K. Furthermore, it was also found that O_2 modulates the photoluminescence of aerogels doped with 4-benzoyl-*N*-methylpyridinium -based dyads over a wider dynamic range compared with aerogels doped with either our viologen-based dyads or with Ru(II) tris(1,10-phenanthroline) itself.

1. Introduction

Oftentimes, the power and versatility of molecule-based chemistry is compromised by the fact that many functional molecules express their useful properties only in solution. For example, photoluminescence from solid samples is usually not observed because it is either self-quenched or self-absorbed. Solutions, however, are not convenient media from a practical standpoint because they raise issues of handling, confinement, and sealing. In that regard, sol−gel glass is an emerging convenient, chemically inert solid matrix for entrapment of functional guests.

Sol−gel glass is a porous material chemically identical to conventional glass, and is derived through the so-called sol−gel process that involves gelation through hydrolysis, condensation, and polymerization of metal and semimetal alkoxides under ambient conditions.[1] Gels resulting from the sol−gel process (hydrogels) can be dried either under ambient pressure yielding xerogels or via supercritical fluid (SCF) extraction (e.g., with CO_2), yielding aerogels.[2] As far as monolithic sol−gel materials are concerned, the SCF drying process is fast compared to ambient pressure drying, and therefore aerogels generally allow rapid prototyping of sol−gel-based platforms for practical applications. But the speed of implementation notwithstanding, aerogels have important properties of their own; since they retain the

* Authors to whom correspondence should be addressed. Tel., (216) 433-3202; e-mail, Nicholas.Leventis@grc.nasa.gov (N. Leventis). Tel., (573) 341-4353; e-mail, cslevent@umr.edu (C. Sotiriou-Leventis).
† NASA Glenn Research Center.
‡ University of Missouri−Rolla.

(1) (a) Brinker, C. J.; Scherer, G. *Sol−Gel Science: the Physics and Chemistry of Sol−Gel Processing*; Academic Press: San Diego, 1990. (b) Hench, L. L.; West, J. K. *Chem. Rev.* **1990**, *90*, 33−72. (c) Dunn, B.; Zink, J. I. *J. Mater. Chem.* **1991**, *1*, 903−913.

(2) (a) Hüsing, N.; Schubert, U. *Angew. Chem., Int. Ed.* **1998**, *37*, 22−45. (b) Pierre, A. C.; Pajonk, G. M. *Chem. Rev.* **2002**, *102*, 4243−4265.

10.1021/cm034999b CCC: $27.50
Published on Web 03/20/2004

volume of the parent hydrogels (but not the pore-filling liquids), they are actually very low-density materials consisting mainly of empty space (referred to as mesoporosity) that can become the host for a variety of functional guests for optical, electronic, and chemical applications.[3] A second benefit of mesoporosity is that it provides molecular species from the environment an almost unobstructed access to entrapped guests, rendering aerogels an ideal support for catalysts and sensors.[4]

A particularly attractive class of functional guests could be dyads of light-harvesting units (LHU) with electron acceptors (or donors). After photoexcitation, these species undergo fast intramolecular electron-transfer quenching, leading transiently to charge separation, and thus they have been considered for optical-to-electrical or optical-to-chemical energy conversion in photovoltaics,[5] and artificial photosynthesis.[6] We have been attracted to LHU-electron acceptor dyads by their possible utility for chemical sensors and optical switches (i.e., modulating light with light).[7] Since there is already a sufficient understanding of the behavior of ruthenium complexes in rigid environments including sol−gel materials,[9] zeolites and polymeric matrixes,[10] the two dyads synthesized for the present study use the Ru(II) tris(1,10-phenanthroline) complex ($[Ru(phen)_3]^{2+}$) as the LHU, linked through ethynyl bridges at the 3- and 8-positions of one of the ligands to either two 4-benzoyl-*N*-methyl pyridinium cations (**1**) or two *N*-benzyl-*N*′-methyl viologen dications (**2**) as the intramolecular quenchers.

The photophysical properties of **1** and **2** were investigated on the silica aerogel surface: (a) in comparison to the corresponding "free bases" **1-FB** and **2-FB**, to elucidate the effect of the presence of the intramolecular quencher vs a more or less invariant structure; (b) in two solvents, to model the impact of the hydroxyl environment of the silanol-rich surface of silica; and (c) in fluid vs frozen environments, to simulate the effect of the environmental rigidity imposed by adsorption on the surface of silica. In terms of environmental rigidity,

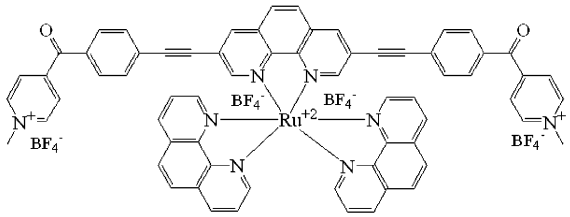

1

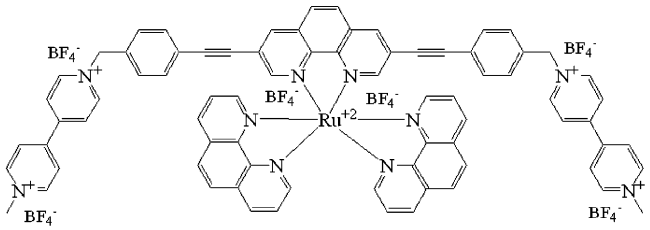

2

the room-temperature photoluminescent properties of aerogels doped with **1** and **2** are similar to those exhibited by the same complexes in frozen solvents at 77 K: upon cooling, the luminescence intensity of the dopant increases and is shifted to the blue, analogous to the typical behavior of Ru(II) polypyridyl complexes in solution. However, the unique property of Ru(II) complex doped aerogels at 77 K in comparison to frozen solutions of the same dopants is that due to their open mesoporous structure, the dopant is still accessible to gas-phase quenchers such as oxygen, a fact which increases the sensitivity of aerogel-based oxygen sensors over the corresponding room-temperature configurations. In that regard, it was also found and is reported herewith that oxygen modulates the photoemission of aerogels doped with **1** over a wider dynamic range than it modulates the photoemission of aerogels doped with **1-FB**, **2-FB**, or **2**.

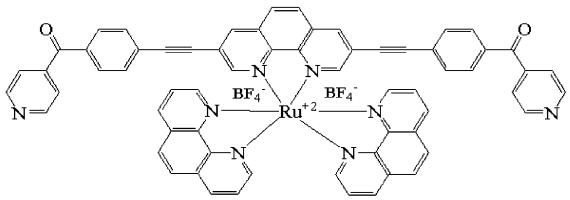

1-FB

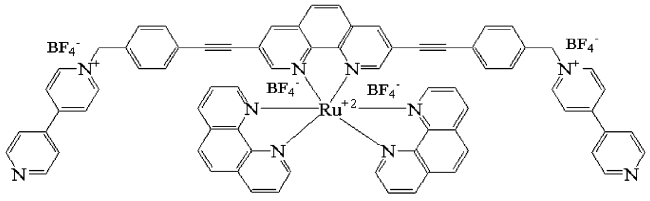

2-FB

2. Results and Discussion

2.1. Design and Synthesis of Ru(II) Complex-Electron Acceptor Dyads 1 and 2. 1,10-Phenanthroline has been used extensively as a bidentate ligand in light-harvesting metal complexes.[11] In terms of substitution, the 3- and 8-positions of this ring system are

(3) Morris, C. A.; Anderson, M. L.; Stroud, R. M.; Merzbacher, C. I.; Rolison, D. R. *Science* **1999**, *284*, 622−624.

(4) Leventis, N.; Elder, I. A.; Rolison, D. R.; Anderson, M. L.; Merzbacher, C. I. *Chem. Mater.* **1999**, *11*, 2837−2845.

(5) Peeters, E.; van Hal, P. A.; Knol, J.; Brabec, C. J.; Sariciftci, N. S.; Hummelen, J. C.; Janssen, R. A. J. *J. Phys. Chem. B* **2000**, *104*, 10174−10190.

(6) (a) Meyer, T. J. *Acc. Chem. Res.* **1989**, *22*, 163−170. (b) Gust, D.; Moore, T. A.; Moore, A. L. *Acc. Chem. Res.* **1993**, *26*, 198−205. (c) Gust, D.; Moore, T. A.; Moore, A. L. *Acc. Chem. Res.* **2001**, *34*, 40−48.

(7) The latter, by taking advantage of the very short-lived transient absorbance of the reduced form of the intramolecular quencher following the photoinduced electron-transfer event, analogous to recent work by Raymo et al. based on merocyanine/spiropyran photochromics.[8]

(8) (a) Giordani, S.; Raymo, F. M. *Org. Lett.* **2003**, *5*, in press. Raymo, F. M.; Alvarado, R. J.; Giordani, S.; Cejas, M. A. *J. Am. Chem. Soc.* **2003**, *125*, 2361−2364. (b) Raymo, F. M.; Giordani, S.; White, A. J. P.; Williams, D. J. *J. Org. Chem.* **2003**, *68*, 4158−4169.

(9) For example see: (a) Momose, F.; Maeda, K.; Matsui, K. *J. Non-Cryst. Solids* **1999**, *244*, 74−80. (b) Innocenzi, P.; Kozuka, H.; Yoko, T. *J. Phys. Chem. B* **1997**, *101*, 2285−2291. (c) Mongey, K. F.; Vos, J. G.; MacCraith, B. D.; McDonagh, C. M.; Coates, C.; McGarvey, J. J. *J. Mater. Chem.* **1997**, *7*, 1473−1479. (d) Castellano, F. N.; Heimer, T. A.; Tandhasetti, M. T.; Meyer, G. J. *Chem. Mater.* **1994**, *6*, 1041−1048. (e) Heimer, T. A.; Bignozzi, C. A.; Meyer, G. J. *J. Phys. Chem.* **1993**, *97*, 11987−11994. (f) Matsui, K.; Sasaki, K.; Takahashi, N. *Langmuir* **1991**, *7*, 2866−2868.

(10) For example see: (a) Maruszewski, K.; Strommen, D. P.; Kincaid, J. R. *J. Am. Chem. Soc.* **1993**, *115*, 8345−8350. (b) Kim, Y.; Mallouk, T. E. *J. Phys. Chem.* **1992**, *96*, 2879−2885. (c) Li, Z.; Wang, C. H.; Persaud, L.; Mallouk, T. E. *J. Phys. Chem.* **1988**, *92*, 2592−2597.

(11) Sammes, P. G.; Yahioglu, G. *Chem. Soc. Rev.* **1994**, *23*, 327−334.

Scheme 1. Synthesis of Ru(II) Complex-Electron Acceptor Dyads

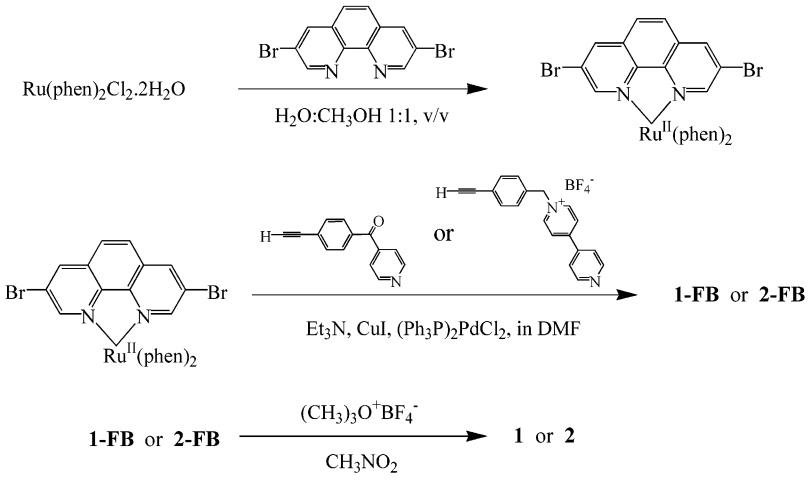

particularly important because they lie along the polarization axis of its most intense electronic transition.[12] So conjugated substituents at those positions would enhance electronic delocalization of the ^{3}MLCT excited state,[13] funneling electron density toward the electron-transfer quenchers.

On the other hand, viologens (diquaternized 4,4′-bipyridinium salts) have been used also extensively as inter-[14] and intramolecular electron-transfer quenchers of Ru(II) complexes.[15] However, the first intramolecular quencher considered for this study was the 4-benzoyl-*N*-methylpyridinium cation: owing to its similar redox chemistry to that of viologen,[16] it is able to quench the ^{3}MLCT photoluminescence of Ru complexes in solution almost as efficiently as viologen (refer to Appendix S.1 in Supporting Information);[17] furthermore, 4-(4-ethynylbenzoyl)pyridine, a key intermediate for the synthesis of **1**, was already available to us from previous studies.[16a] Conversely, synthesis of **2** would require preparation of several new intermediates. Nevertheless, as it will become apparent below, certain photoluminescent properties of **1** were rather unexpected, and thus synthesis of **2** became necessary not only because it is a molecule inherently relevant to this study but also as an internal reference for the properties of **1**.

Historically, 3,8-disubstituted 1,10-phenanthrolines had been more difficult to synthesize than their 2,9- or 4,7-analogues,[18] until Tor and co-workers demonstrated an efficient one-step non-Skraup-type procedure for the preparation of 3-bromo and 3,8-dibromo-1,10-phenantholine by direct bromination of the HCl salt of 1,10-phenanthroline.[19] Tor has also shown that the reactivity of those compounds toward Sonogashira-type coupling reactions can be enhanced significantly by coordination.[20] Thus, according to Tor's procedure, 3,8-dibromo-1,10-phenanthroline coordinated to Ru(II) was coupled uneventfully either with 4-(4-ethynylbenzoyl)pyridine to yield **1-FB** or with *N*-(4-ethynylbenzyl)-4,4′-bipyridinium tetrafluoroborate to yield **2-FB**. Quaternization of **1-FB** and **2-FB** with $(CH_3)_3O^+BF_4^-$ yields **1** and **2**. The general synthetic procedure is summarized in Scheme 1. For experimental details and compound identification data refer to the Experimental Section; ^{1}H NMRs and representative mass spectra are shown in Appendix S.2 of the Supporting Information; the synthesis of *N*-(4-ethynylbenzyl)-4,4′-bipyridinium tetrafluoroborate is summarized in Appendix S.3.

2.2. Photophysical Characterization of 1, 1-FB, 2 and 2-FB in Fluid Solution at Room Temperature. All electronic absorption spectra are shown in Figure 1 (The expanded long wavelength region of the same absorption spectra is given in Appendix S.4.) By comparison with $[Ru(phen)_3]^{2+}$, we note that all new complexes show an additional broad shoulder in the 270−300 nm region, a strong absorption band in the 325−400 nm region, and a new weaker absorption band in the 475−525 nm range. By comparison of the absorption spectra of **1** and **1-FB** to the spectrum of the free ligand **3** (Figure 2),[21] the additional absorption features

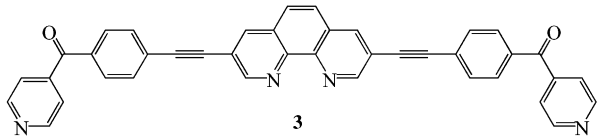

3

of the complexes in the UV are assigned to the new internal ligand transitions. Similarly, the long-wave-

(12) Bosnich, B. *Acc. Chem. Res.* **1969**, *2*, 266−273.
(13) Joshi, H. S.; Jamshidi, R,; Tor, Y. *Angew. Chem, Int. Ed.* **1999**, *38*, 2722−2725.
(14) Wasielewski, M. R. *Chem. Rev.* **1992**, *92*, 435−461.
(15) For recent examples see: (a) Martre, A.; Laguitton-Pasquier, H.; Deronzier, A.; Harriman, A. *J. Phys. Chem. B* **2003**, *107*, 2684−2692. (b) Schild, V.; van Loyen, D.; Durr, H.; Bouas-Laurent, H.; Turro, C.; Worner, M.; Pokhrel, M. R.; Bossmann, S. H. *J. Phys. Chem. A* **2002**, *106*, 9149−9158.
(16) (a) Leventis, N.; Elder, I. A.; Gao, X.; Bohannan, E. W.; Sotiriou-Leventis, C.; Rawashdeh, A.-M. M.; Overschmidt, T. J.; Gaston, K. R. *J. Phys. Chem. B* **2001**, *105*, 3663−3674. (b) Leventis, N.; Rawashdeh, A.-M. M.; Zhang, G.; Elder, I. A.; Sotiriou-Leventis, C. *J. Org. Chem.* **2002**, *67*, 7501−7510. (c) Leventis, N.; Zhang, G.; Rawashdeh, A.-M. M.; Sotiriou-Leventis, C. *Electrochim. Acta* **2003**, *48*, 2799−2806.
(17) For a study of the quenching properties of other related pyridinium systems see: Jones, G., II; Malba, V.; *J. Org. Chem.* **1985**, *50*, 5776−5782.
(18) (a) Ziessel, R.; Suffert, J.; Youinou, M.-T. *J. Org. Chem.* **1996**, *61*, 6535−6546. (b) Suffert, J.; Ziessel, R. *Tetrahedron Lett.* **1991**, *32*, 757−760. (b) Schmittel, M.; Ammon, H. *Eur. J. Org. Chem.* **1998**, *785*, 5−792. (c) Case, F. H. *J. Am. Chem. Soc.* **1948**, *70*, 3994−3996. (d) Case, F. H. *J. Org. Chem.* **1951**, *16*, 941−945.
(19) (a) Tzalis, D.; Tor, Y.; Failla, S.; Siegel, J. S. *Tetrahedron Lett.* **1995**, *36*, 3489−3490. (b) Saitoh, Y.; Koizumi, T.; Osakada, K.; Yamamoto, T. *Can. J. Chem.* **1997**, *75*, 1336−1339.
(20) Tzalis, D.; Tor, Y. *Angew. Chem., Int. Ed. Engl.* **1997**, *36*, 2666−2668.
(21) Yang, J.; Oh, W. S.; Elder, I. A.; Leventis, N.; Sotiriou-Leventis, C. *Synth. Commun.* **2003**, *33*, 3317−3325.

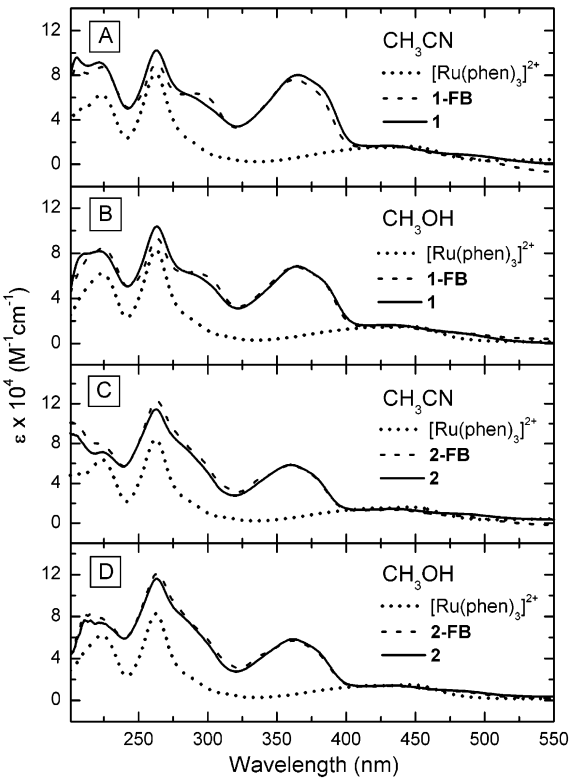

Figure 1. Absorption spectra of Ru(II) complexes in solution at room temperature. A: [**1**] = 9.95 × 10^{-6} M; [**1-FB**] = 9.65 × 10^{-6} M; [[Ru(phen)$_3$]$^{2+}$] = 1.20 × 10^{-5} M. B: [**1**] = 1.66 × 10^{-5} M; [**1-FB**] = 1.45 × 10^{-5} M; [[Ru(phen)$_3$]$^{2+}$] = 2.40 × 10^{-5} M. C: [**2-FB**] = 1.16 × 10^{-5} M; [**2**] = 1.39 × 10^{-5} M. D: [**2-FB**] = 1.15 × 10^{-5} M; [**2**] = 1.16 × 10^{-5} M.

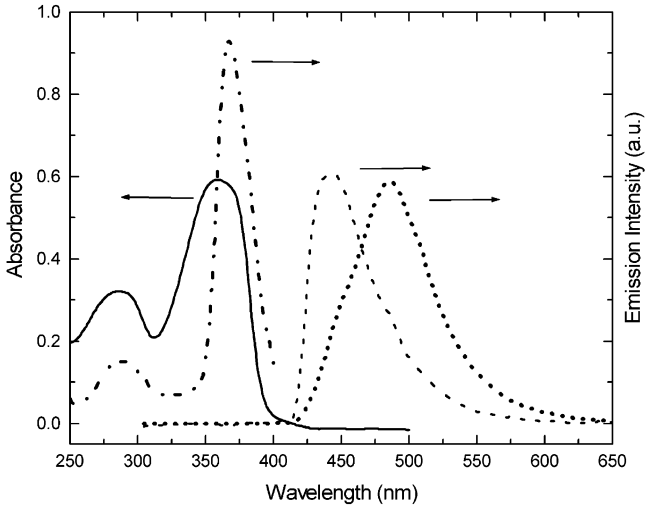

Figure 2. Absorption (—, 1 cm path length; conc. = 1.303 × 10^{-5} M), emission at room temperature (- - -, λ_{max} = 442 nm, τ ~ 4 ns), emission at 77 K (···, λ_{max} = 486 nm, τ ~ 13 ns), and excitation spectrum at room temperature (-·-·-, λ_{ex} = 440 nm) of free ligand **3** in $CHCl_3$.

length absorption features in the visible are assigned to the new MLCT transitions to the substituted 1,10-phenanthroline ligands. It is worth noting that the absorption spectra of **1** and **1-FB** are not only similar to one another but also practically identical to the spectra of **2** and **2-FB**. This implies that the extent of ligand delocalization in the two sets of complexes is also very similar, irrespective of the groups attached to the other end of the ethynyl bridges. This view is supported by molecular orbital calculations showing a metal-centered HOMO, and a LUMO with no significant electron density in the phenyl groups beyond the ethynyl bridges (see Supporting Information, Appendix S.5).

All emission data are summarized in Table 1 and include excited-state lifetimes and selected quantum yields. Figure 3 compares the room-temperature emission spectra of **1**, **1-FB**, **2**, and **2-FB** with the emission spectra of [Ru(phen)$_3$]$^{2+}$. As expected, both **1-FB** and **2-FB** are photoluminescent, and their emission spectra are red-shifted by ~70 nm relative to those of [Ru(phen)$_3$]$^{2+}$ in the same solvents; in CH_3CN the emission spectra of the same two compounds are slightly red-shifted (~4−7 nm) relative to their emission in methanol or ethanol. The photoluminescence of **1-FB** and **2-FB** is attributed to ^{3}MLCT transitions from modified 1,10-phenanthroline ligands. This assignment is supported both by the absorption data and by the localization of the LUMO on the larger ligand (Appendix S.5). In the case of **1-FB**, where the ligand (**3**) has been synthesized independently,[21] it is confirmed by comparison of Figures 2 and 3B that no internal-ligand emission is observed.

Compound **1** does not emit in CH_3CN and compound **2** does not emit either in CH_3CN or CH_3OH. Surprisingly, however, **1** *does* emit in methanol (and ethanol).

A different perspective into the photoluminescent properties of the complexes of this study is obtained through emission lifetimes and quantum yields. At room temperature, the emission lifetime of [Ru(phen)$_3$]$^{2+}$ is in the range of 0.2−0.3 μs, while the lifetimes of **1-FB** and **2-FB** are significantly longer (1.5−1.8 μs). Since the lifetime of an excited state in a particular matrix is a "fingerprint" property, the fact that the lifetimes of **1-FB** and **2-FB** are in the same range (in comparison with the lifetime of [Ru(phen)$_3$]$^{2+}$), corroborates further the view that the excited states of the two complexes are very similar. Now, compound **2** is not photoluminescent in solution, implying that the rate of intramolecular electron transfer, k_{ET}, is much greater than $1/\tau_{\mathbf{2-FB}}$, or $k_{ET} \gg 6.7 \times 10^5$ s^{-1}. On the other hand, the relative room-temperature emission quantum yields of [Ru(phen)$_3$]$^{2+}$, **1-FB,** and **1** in ethanol are 1:0.77:0.30, respectively. Given that the radiative and radiationless rate constants k_r and k_d, respectively, are related to the corresponding emission quantum yields and lifetimes by $\Phi = k_r \times \tau$ and $k_r + k_d = \tau^{-1}$, it is possible to calculate the values of k_r and k_d wherever quantum yield and lifetime data are available (Table 2). Thus, we see that the main reason for the reduced emission quantum yields of **1** and **1-FB** relative to that of [Ru(phen)$_3$]$^{2+}$ is a more substantial drop in k_r rather than in k_d. By looking more closely, it is also noted that by going from **1-FB** to **1** in ethanol, the value of k_d remains practically unchanged, implying that the presence of the 4-benzoyl-*N*-methylpyridinium cation adds no extra deactivation pathways in that solvent. In other words, it appears that, for **1** in alcohol, $k_{ET} \sim 0$.

2.3. Photophysical Characterization of 1, 1-FB, 2, and 2-FB in Frozen Matrixes at 77 K. In frozen matrixes (77 K) of the same solvents as above (methanol, ethanol, and CH_3CN), all four complexes are photoluminescent (Figure 4), and wherever a direct comparison is possible, the spectra are intensified and blue-

Table 1. Emission Wavelength Maxima (λ_{max}) and Excited State Lifetimes (τ) for 1, 1-FB, $[Ru(phen)_3]^{2+}$, 2-FB, and 2 in Solution, in Frozen Matrix at 77 K, and on Silica Aerogel Both at Room Temperature and at 77 K; Selected Emission Quantum Yield Data (Φ) Are Also Included

	solvent	complex **1** λ_{max}, nm [τ, ns]	complex **1-FB** λ_{max}, nm [τ, ns]	$[Ru(phen)_3]^{2+}$ λ_{max}, nm [τ, ns]	complex **2-FB** λ_{max}, nm [τ, ns]	complex **2** λ_{max}, nm [τ, ns]
RT	CH_3CN	*a*	**672** [1515 ± 12], $\Phi = 0.027$[d]	**594** [327 ± 3], $\Phi = 0.050$[d]	**665** [1811 ± 12], $\Phi = 0.029$[d]	*a*
	CH_3OH	**653** [1760 ± 18]	**669** [1350 ± 12]	**597** [220 ± 2]	**658** [1805 ±11]	*a*
	ethanol	**655** [1457 ± 35], $\Phi = 0.014$[d]	**662** [1552 ± 14], $\Phi = 0.036$[d]	**598** [172 ± 2], $\Phi = 0.047$[d]	**656** [1498 ± 26], $\Phi = 0.036$[d]	*a, b*
77 K	CH_3CN	**660** [378 ± 14 (57%), 2498 ± 65 (43%)]	**661** [266 ± 16 (52%), 2526 ± 104 (48%)]	**585** [531 ± 19 (51%), 5293 ± 122 (49%)]	**645** [303 ± 27 (48%), 3571 ± 112 (52%)]	**642** [493 ± 32 (48%), 3846 ± 134 (52%)]
	CH_3OH	**632** [5506 ± 50]	**641** [5095 ± 62]	**574** [10030 ± 65]	**629** [4960 ± 35]	**629** [5322 ± 69]
	ethanol	**633** [5468 ± 47]	**640** [5043 ± 60]	**573** [9571 ± 53]	**630, 685$_{sh}$** [5757 ± 74]	*a, b*
aerogel at RT[c]		**643** [280 ± 15 (40%), 2400 ± 37 (60%)]	**643** [434 ± 55 (29%), 2763 ± 67 (71%)]	**604** [237 ± 11 (60%), 2308 ± 71 (40%)]	**639** [439 ± 31 (45%), 2824 ± 71 (55%)]	**640** [416 ± 31 (38%), 2706 ± 58 (62%)]
aerogel at 77 K[c]		**622** [910 ± 69 (14%), 10736 ± 127 (86%)]	**625** [2169 ± 220 (21%), 9676 ± 200 (79%)]	**594** [14925 ± 145]	**615** [257 ± 78 (13%), 11462 ± 227 (87%)]	**620** [125 ± 23 (1%), 8968 ± 148 (99%)]

[a] No observable emission at room temperature. [b] Low solubility. [c] Samples degassed and flame-sealed under vacuum. [d] Emission quantum yields were calculated according to ref 13, using the emission quantum yield of $[Ru(2,2'\text{-bipyridine})_3]^{2+}$ in water at 25 °C ($\Phi = 0.041$) as reference.[22]

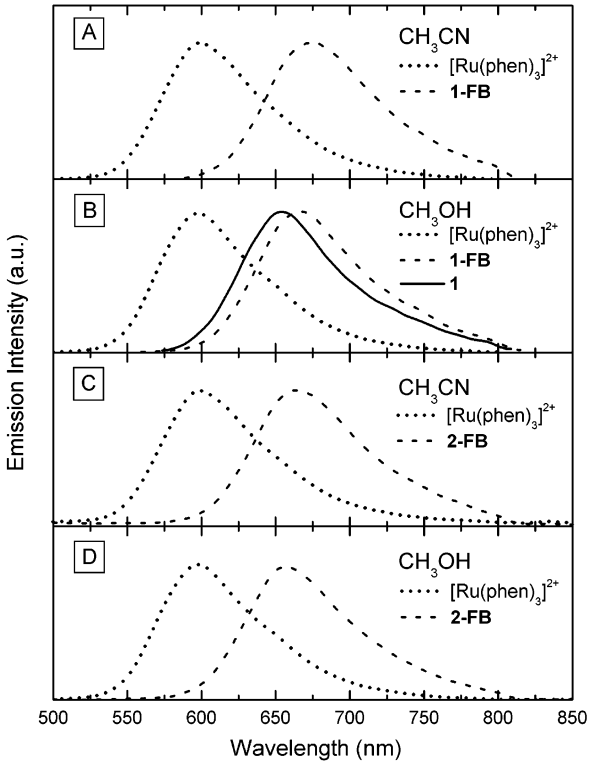

Figure 3. Room-temperature emission spectra of the Ru(II) complexes in solution. Complex concentrations ~ 10^{-4} M. Both complexes **1** and **2** show no observable emission in CH_3CN. Complex **2** shows no observable emission in CH_3OH either. Spectra have been scaled for clarity; relative intensities are arbitrary.

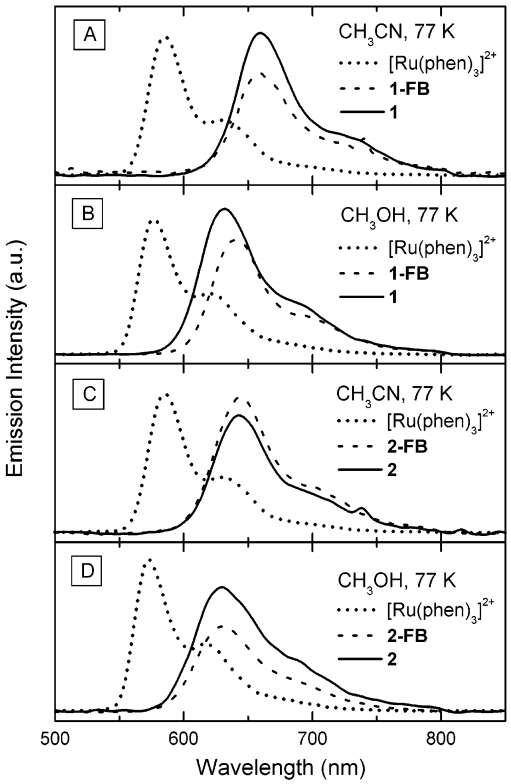

Figure 4. Emission spectra of the Ru(II) complexes in frozen solvent matrix at 77 K. Complex concentrations ~ 10^{-4} M. All complexes emit in both matrixes. Spectra have been scaled for clarity; relative intensities are arbitrary.

Table 2. Room-Temperature Radiative and Radiationless Rate Constants (k_r and k_d) for $[Ru(phen)_3]^{2+}$, 1-FB, 1, and 2-FB in Solution

	CH_3CN		ethanol	
	k_r, s^{-1}	k_d, s^{-1}	k_r, s^{-1}	k_d, s^{-1}
$Ru(phen)_3]^{2+}$	1.5×10^5	1.9×10^6	2.7×10^5	5.5×10^6
1-FB	1.8×10^4	6.4×10^5	2.3×10^4	6.2×10^5
1	9.6×10^3	6.8×10^5		
2-FB	1.6×10^4	5.4×10^5	2.4×10^4	6.4×10^5

shifted (by 9−29 nm) relative to their fluid solvent counterparts. Furthermore, the observed differences in the λ_{max} for any given complex between frozen CH_3CN and frozen CH_3OH are larger (9−28 nm) than the corresponding differences in solution (3−7 nm). It should also be noted that consistently the smaller wavelength changes in any given range correspond to $[Ru(phen)_3]^{2+}$ itself, while the values for **1**, **1-FB**, **2**, and **2-FB** are segregated closer to the upper end of the corresponding range. Thus, in frozen CH_3CN the emission spectra of **1** and **1-FB** are practically identical and red-shifted by 27 and 22 nm, respectively, relative to their emission maxima in frozen CH_3OH. In the case of **2** and **2-FB**, the emission spectra are also very close to one another ($\Delta\lambda_{max} = 0-3$ nm), and again the spectra of **2** and **2-FB** are red-shifted in frozen CH_3CN by 12 and 15 nm, respectively, relative to their spectra in frozen CH_3OH. The low-temperature emission decay of

all complexes in frozen CH_3CN is biexponential and consists of two components with about equal contributions: a short-lived one (0.3−0.5 μs) and a long-lived one (3−5 μs). In frozen methanol or ethanol matrixes, we observe consistently only one long-lived exponential decay (∼5 μs) for all complexes.

The low-temperature enhancement in both the emission intensity and lifetime is understood in terms of the well-documented mechanism for radiationless decay of the ^{3}MLCT excited state of Ru(II) tris(bidentate ligand) complexes via thermal population of the higher in energy ^{3}dd state:[23] In the frozen matrix not only thermal population of the ^{3}dd state is less favorable, but also the rigid environment restricts the low-frequency Ru−N vibrations. Since the amplitude of those vibrations needs to increase upon population of the ^{3}dd state, the energy of that state is pushed to higher energy.[24] On the other hand, the blue shift of the emission spectra occurring during the fluid-to-rigid matrix transition has been known as the regidochromic effect,[25] and again it is attributed to the restrictions imposed by the rigid environment on both the increase in the average internuclear distance in the excited state and on the reorientation of the (polar) solvent molecules in response to the redistribution of charge in the excited state.[24c] Now, in addition to the regidochromic effect, the restricted solvent reorientation by the frozen environment has other important consequences as well: it inhibits intramolecular electron-transfer quenching in both **1** and **2** by preventing solvation (and therefore stabilization) of the species that would be produced from the electron-transfer event. The importance of those solvation effects (or the lack thereof) is indicated by the augmented sensitivity of the emission spectrum on the chemical identity of the frozen matrix at 77 K, as compared to the room-temperature spectrum. In Marcus theory terms, the solvent reorganization energy that is lost in the frozen environment is larger than the Gibbs free enthalpy change during the quenching event.[26]

2.4. Redox Characterization of 1, 1-FB, 2, and 2-FB. The spectroscopic properties of the Ru(II) dyads in alcohols were studied as a model for the behavior of **1** and **2** on the silanol-terminated surface of silica aerogels.[27] Thus, while the spectroscopic properties of **2** in alcohol agree with what we would have expected for a Ru(II) complex/electron acceptor dyad both in solution and in frozen matrix, the presence of a strong room-temperature photoluminescence from **1** in methanol (and ethanol) was surprising. Meanwhile, electrochemistry allows evaluation of the relative energy levels of the orbital responsible for the MLCT emission and

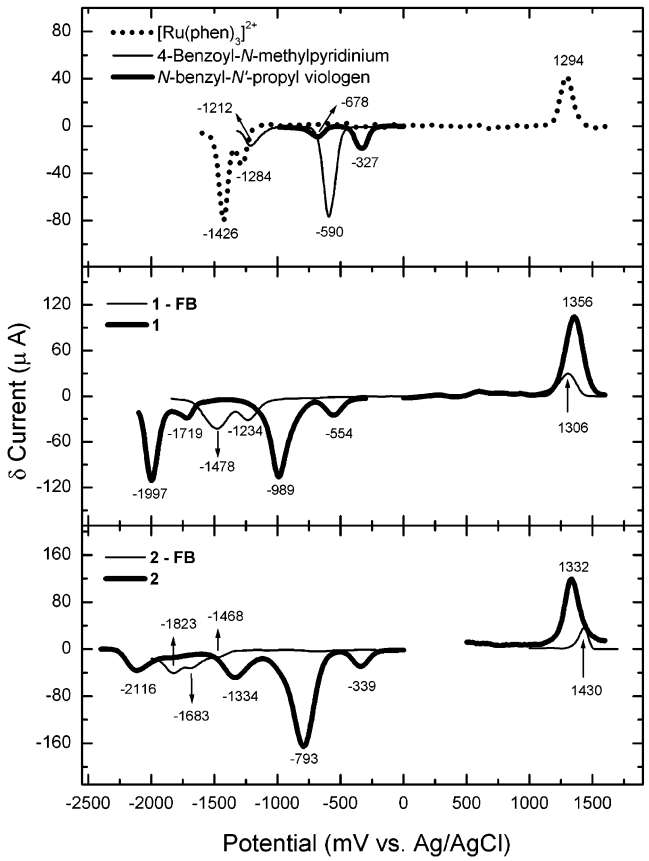

Figure 5. Differential pulse voltammetry (DPV: pulse height = 50 mV; pulse width = 50 ms; scan rate = 5 mV s^{-1}; scan increment: 5 mV; step time = 1 s) in Ar-degassed CH_3CN/0.1 M TBAP with a Au disk electrode (1.6 mm in diameter). [[Ru(phen)$_3$]$^{2+}$] = 1.66 mM, [**1**] = 1.51 mM, and [**1-FB**] = 1.43 mM, [**2**] = 0.9 mM, [**2-FB**] = 1.05mM, [4-benzoyl-*N*-methylpyridinium tetrafluoroborate] = 7.00 mM, [*N*-benzyl-*N*′-propyl viologen bis tetrafluoroborate] = 2.20 mM.

the "LUMO" of the intramolecular quencher. Thus, the investigation of the sharp contrast in the room-temperature photoluminescent behavior of **1** and **2** in CH_3CN and alcohol led naturally to a comparative study of the solvent effect on the redox behavior of all complexes and of the two quenchers, namely, the 4-benzoyl-*N*-methylpyridnium cation and *N*-benzyl-*N*′-propyl viologen. Figures 5 and 6 show the differential pulse voltammograms of these quenchers in CH_3CN and CH_3OH, respectively. In both figures, part A shows the electrochemical behavior of [Ru(phen)$_3$]$^{2+}$ and of the two intramolecular quenchers; part B compares the behavior of **1-FB** and **1**; and part C concerns **2-FB** and **2**.[28] As shown in Figure 5A, all reductions of both quenchers take place at less negative potentials than all reductions of [Ru(phen)$_3$]$^{2+}$. Furthermore, the first electron reduction of 4-benzoyl-*N*-methyl pyridinium cation (−578 mV vs Ag/AgCl) falls between the two 1-e reduction waves of *N*-benzyl-*N*′-propyl viologen (−327 and −678 mV vs Ag/AgCl, respectively). Practically, the same sequence prevails in CH_3OH (Figure 6A); and although H-bonding between the 2-e reduced form of the 4-benzoyl-*N*-

(22) Van Houten, J.; Watts, R. J. *J. Am. Chem. Soc.* **1976**, *98*, 4853−4858.

(23) (a) Hipps, K. W.; Crosby, G. A. *J. Am. Chem. Soc.* **1975**, *97*, 7042−7048. (b) Meyer, T. J. *Pure Appl. Chem.* **1990**, *62*, 1003−1009. (c) Macatangay, A.; Zheng, G. Y.; Rillema, D. P.; Jackman, D. C.; Merkert, J. W. *Inorg. Chem.* **1996**, *35*, 6823−6831.

(24) (a) Gardner, P. J.; Kasha, M. *J. Chem. Phys.* **1969**, *50*, 1543−1552. (b) Dellinger, B.; Kasha, M. *Chem. Phys. Lett.* **1975**, *36*, 410−414. (c) Barigelletti, F.; Belser, P.; von Zelewski, A.; Juris, A.; Balzani, V. *J. Phys. Chem.* **1985**, *89*, 3680−3684.

(25) Wrighton, M.; Morse, D. L. *J. Am. Chem. Soc.* **1974**, *96*, 998−1003.

(26) Chen, P.; Danielson, E.; Meyer, T. J. *J. Phys. Chem.* **1988**, *92*, 3708−3711.

(27) See for example: Mongey, K. F.; Vos, J. G.; MacCraith, B. D.; McDonagh, C. M.; Coates, C.; McGarvey, J. J. *J. Mater. Chem.* **1997**, *7*, 1473−1479.

(28) Differential pulse voltammetry (DPV) provides good resolution with closely spaced waves such as those in the redox response of most complexes involved in this study. The position of the maximum δCurrent value is located at $E_{1/2} - \Delta E/2$ (whereas ΔE is the pulse height, and it was set at 50 mV for all experiments.[29]

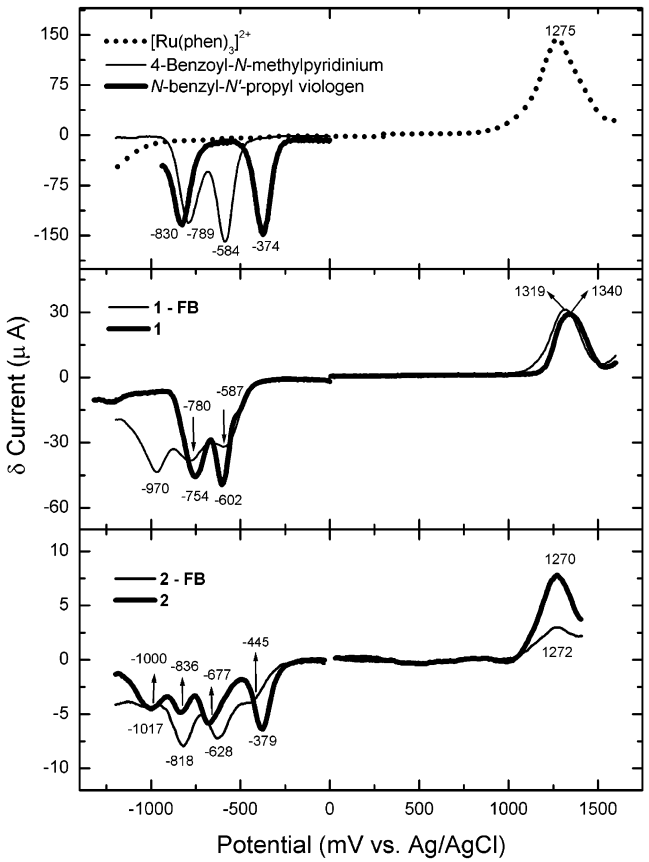

Figure 6. Differential pulse voltammetry in Ar-degassed CH_3OH/0.1 M TBAP. Other experimental conditions as in Figure 5. [4-Benzoyl-*N*-methylpyridinium tetrafluoroborate] = 7.7 mM, [*N*-benzyl-*N*′-propyl viologen bis tetrafluoroborate] = 2.16 mM (current scale times 10). The ruthenium complexes demonstrate poor solubility in CH_3OH and their concentration is in the 0.1 mM range.

methylpyridinium cation and CH_3OH shifts the second reduction wave closer to the first one, nevertheless, the 1st-e reduction of 4-benzoyl-*N*-methylpyridinium cation (−584 mV) is still more negative than the 1st-e reduction of *N*-benzyl-*N*′-propyl viologen (−374 mV). Again, all reductions of both quenchers are still easier than reduction of $[Ru(phen)_3]^{2+}$.

Now back in CH_3CN, the redox characteristics of both **1-FB** (Figure 5B, thin line) and **2-FB** (Figure 5C, thin line) are qualitatively similar to those of $[Ru(phen)_3]^{2+}$, whose 1st-e reduction places an electron in the ligand π^*.[30] Thus, **1-FB** shows two reduction waves with the same 2:1 δCurrent ratio, and in about the same potential range as the waves from $[Ru(phen)_3]^{2+}$. **2-FB** shows an additional wave that is attributed to the reduction of the monoquaternized *N*-benzyl-4,4′-bipyridinium cation. Quaternization of the free pyridines and transformation of **1-FB** and **2-FB** into **1** and **2**, respectively, changes the redox behavior of the complexes dramatically, first by shifting the reduction of the substituted 1,10-phenanthroline ligand to less negative potentials (to −989 and −793 mV for **1** and **2**, respectively), and second by introducing the reduction waves of the intramolecular quencher. Importantly, however, in both complexes **1** and **2** reduction of the corresponding quencher remains easier than reduction of the ligand: the 4-benzoyl-*N*-methylpyridinium group in **1** is reduced at −554 mV vs Ag/AgCl, while *N*-benzyl-*N*′-methyl viologen in **2** is reduced at −339 mV vs Ag/AgCl. Therefore, in both **1** and **2**, it is favorable energetically for an electron promoted by MLCT photoexcitation into the LUMO (π^*) of the 3,8-disubsituted 1,10-phenanthroline to hop subsequently into the quencher. As a result, neither **2** nor **1** are photoluminescent in CH_3CN.

In methanol, we observe that all reduction waves of both free bases, **1-FB** and **2-FB**, have been shifted to less negative potentials. It is also noteworthy that in contrast to CH_3CN, where the redox potentials of **1-FB** (Figure 5B, thin line) are very similar to those of $[Ru(phen)_3]^{2+}$, in CH_3OH (Figure 6B, thin line) the reduction of the ligand is much easier. Qualitatively, similar observations can be made for **2-FB** (refer to Figures 5C and 6C, thin lines), although in this case the presence of the monoquaternized *N*-benzyl-4,4′-bipyridinium cation yields voltammograms more complicated than those of **1-FB.** All potential shifts in the positive direction are traceable to solvation effects by alcohol of both the 1,10-phenanthroline ligand itself, and its 1-e reduced form, analogous to well-documented studies of the redox chemistry of quinones,[31] and of the 4-benzoyl-*N*-methylpyridinium system.[16] After quaternization of **2-FB**, the first redox wave of the *N*-benzyl-*N*′-methyl viologen group in the resulting **2** (−379 mV vs Ag/AgCl) remains at more positive potentials (lower in energy) than the first reduction of the substituted 1,10-phenanthroline, and therefore electron hopping to the quencher is still energetically favorable, just as in CH_3CN. Consequently, photoemission from **2** in alcohols is not observed. On the other hand, after quaternization of **1-FB**, the 1st-e reduction of the 4-benzoyl-*N*-methylpyridinium group in the resulting **1** overlaps with the reduction of the substituted 1,10-phenanthroline ligand; thus, electron hopping is energetically less favorable than in the case of **2**. From a Marcus perspective, this means that the rate of electron transfer from the ^{3}MLCT excited state to the 4-benzoyl-*N*-methylpyridinium cation is expected to be slower in alcohols than is acetonitrile.

2.5. Preparation and Spectroscopic Characterization of Silica Aerogel Monoliths, Doped with 1, 2, 1-FB, 2-FB, and $[Ru(phen)_3]^{2+}$. Monolithic silica hydrogels (radius ∼ 1 cm; length ∼ 3 cm) were prepared from tetramethoxysilane in methanol via a base-catalyzed route.[4] The resulting gels were aged and washed extensively with methanol and water. Detailed procedures for post-gelation doping with **1**, **2**, **1-FB**, **2-FB**, and $[Ru(phen)_3]^{2+}$ are described in the Experimental Section. Hydrogels prepared by a base-catalyzed route are expected to have a negatively charged surface.[32] Binding of the positively charged Ru(II) complexes is then electrostatic, and no leaching was observed in any of the subsequent solvent washings, or the extractions with SCF CO_2 in the autoclave. The apparent concentration of the Ru(II) complex in the aerogel monoliths is $\sim 8.5 \times 10^{-5}$ M, corresponding to

(29) Bard, A. J.; Faulkner, L. J. *Electrochemical Methods, Fundamentals and Applications, 2nd ed.*; Wiley: New York, 2000.
(30) Tokel-Takvoryan, N. E.; Hemingway, R. E.; Bard, A. J. *J. Am. Chem. Soc.* **1973**, *95*, 6582−6589.
(31) Gupta, N.; Linschitz, H. *J. Am. Chem. Soc.* **1997**, *119*, 6384−6391.
(32) Wallace, W.; Hoggard, P. *Inorg. Chem.* **1980**, *19*, 2141−2145.

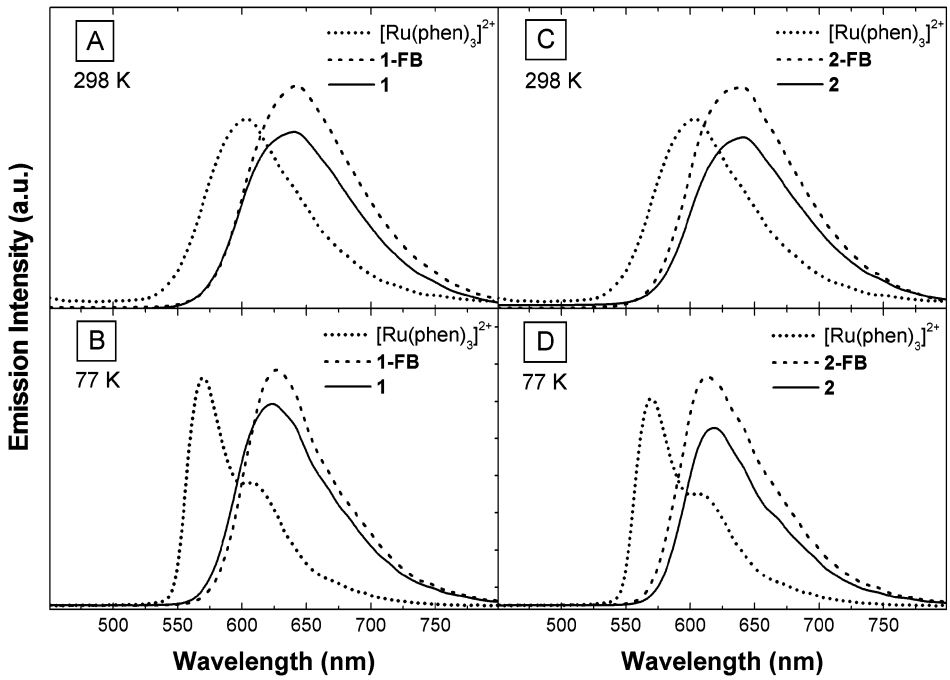

Figure 7. Emission spectra at room temperature and at 77 K of aerogels doped with $[Ru(phen)_3]^{2+}$, **1**, and **1-FB** (A and B) and of aerogels doped with $[Ru(phen)_3]^{2+}$, **2**, and **2-FB** (C and D). Spectra have been scaled for clarity; relative intensities are arbitrary.

1/2000 of a monolayer coverage (given that the surface area of our native aerogels is ~1000 $m^2\ g^{-1}$).[33]

The photoluminescent behavior both at room temperature and at 77 K of aerogels doped with **1**, **1-FB**, **2**, **2-FB**, and $[Ru(phen)_3]^{2+}$ is shown in Figure 7 and is summarized in Table 1. All doped aerogels are photoluminescent at both temperature extremes. The emission spectra of dyad-doped aerogels are red-shifted with respect to those doped with $[Ru(phen)_3]^{2+}$. At room temperature, all four **1-FB**, **1**, **2-FB**, and **2** show practically identical emission maxima (in the 639−643 nm range) with biexponential emission decays consisting of a short-lived component (0.28−0.44 μs) and a long-lived one (2.4−2.7 μs), whose relative contributions range between 29% and 45% and 71% and 55%, respectively. (Typical emission decay data and the fitting curves are shown in Supporting Information, Appendix 5.6.) Upon cooling in liquid N_2 as described in the Experimental Section, the emission is intensified and is shifted to the blue. These phenomena are demonstrated in Figure 8A by **1**, whose emission intensity increases by a factor of "4" and its λ_{max} shifts by 21 nm to the blue. In turn, Figure 8B compares the final emission spectrum of **1** at 77 K with its emission in frozen methanol and shows that in the aerogel at 77 K the emission maximum is blue-shifted by 10 nm relative to the emission in frozen methanol. Similar blue shifts between aerogel at 77 K and frozen methanol are also observed for **1-FB**, **2**, and **2-FB**; for **1-FB** the blue shift is 16 nm, 14 nm for **2-FB**, and 9 nm for **2** (the actual spectra are shown in Appendix S.7). At low temperature, the emission decays are still biexponential; in the cases of **1** and **1-FB**, the lifetimes of both the short- and long-lived components have become significantly longer (Table 1). In the cases of **2** and **2-FB**, the lifetime of the short-lived component has become somewhat shorter.

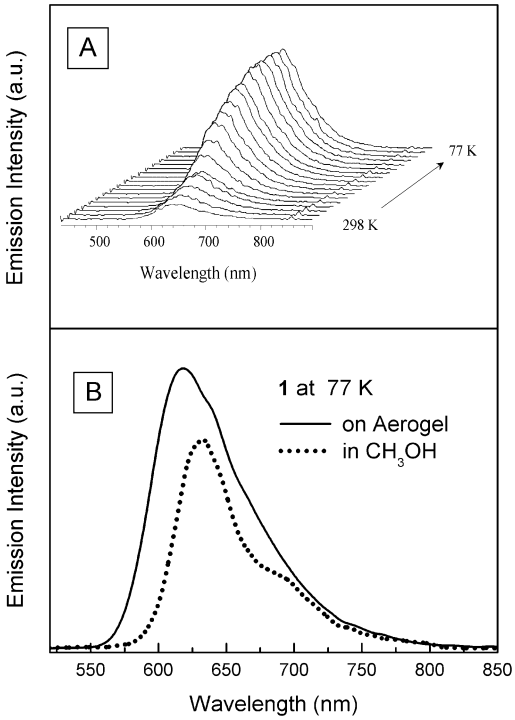

Figure 8. (A) Emission change of a silica aerogel doped with **1** as it has been cooled from room temperature to 77 K under nitrogen. (B) Comparative emission spectra of **1** at 77 K on a silica aerogel and in frozen methanol matrix. Spectra have been scaled for clarity; relative intensities are arbitrary.

In all cases, the contribution of the long-lived component dominates the emission output, with contributions ranging from 79% (for **1-FB**) to 100% (for $[Ru(phen)_3]^{2+}$).

The fact that in alcohol ligand **3** and its reduced forms in both **1-FB** and **1** are stabilized by solvation (vide ante) complicates matters to the point that the lack of room-temperature intramolecular quenching by 4-benzoyl-*N*-methylpyridinium when **1** is immobilized on silica cannot be associated firmly either with the

(33) Leventis, N.; Sotiriou-Leventis, C.; Zhang, G.; Rawashdeh, A.-M. M. *Nano Lett.* **2002**, *2*, 957−960.

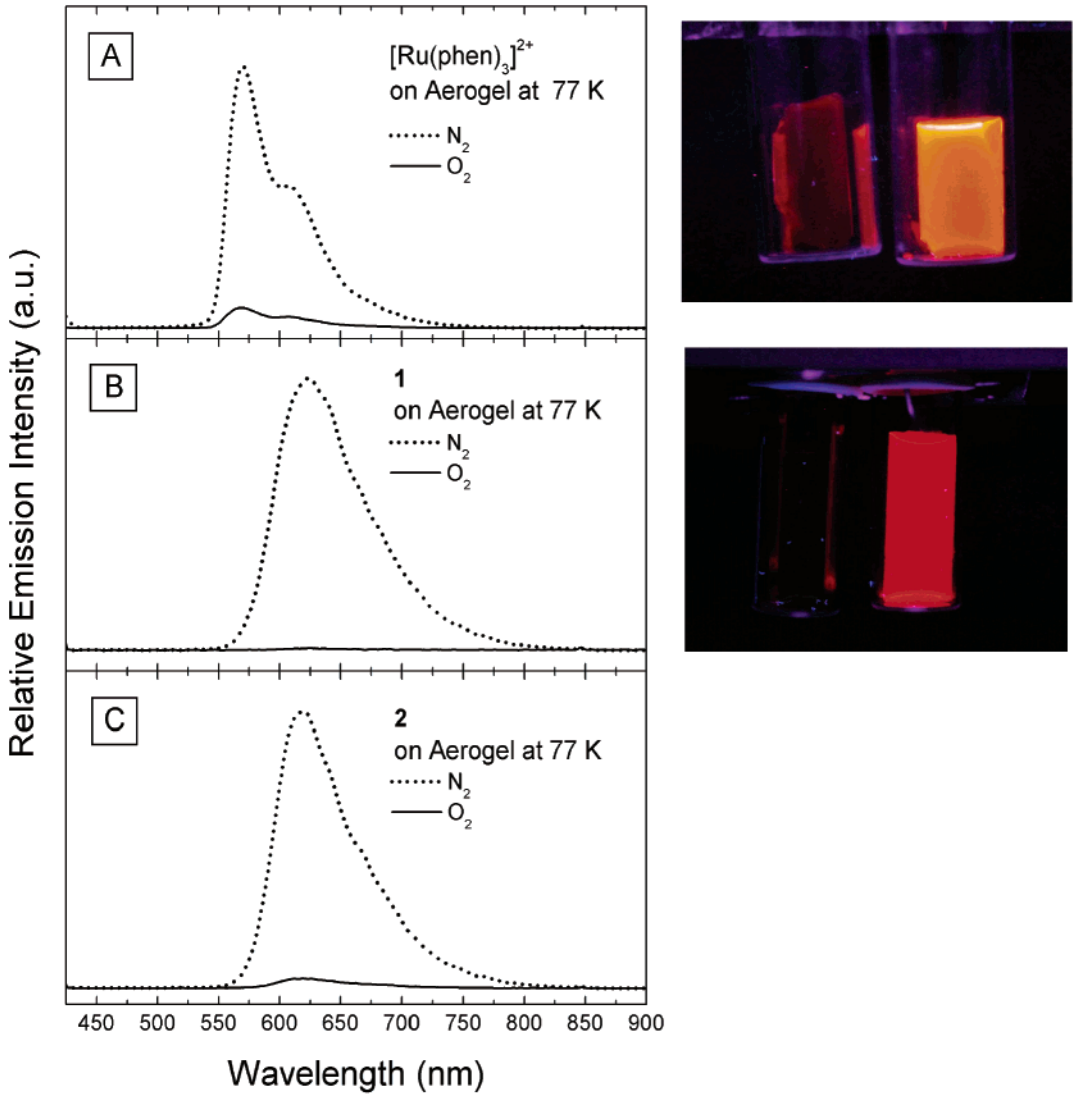

Figure 9. Differences in the emission spectra at 77 K of silica aerogels doped with $[Ru(phen)_3]^{2+}$ (A), **1** (B), and **2** (C) under nitrogen and under oxygen. Photographs on the right demonstrate that, at room temperature as well, a pure oxygen environment quenches the photoemission of aerogels doped with **1** more efficiently than it quenches the photoemission of aerogels doped with $[Ru(phen)_3]^{2+}$.

environmental rigidity or with possible surface solvation effects. In the case of **2**, however, no unusual solvation effects were observed electrochemically in alcohol, and therefore the presence of room-temperature photoemission from **2** immobilized on silica implies that the environmental rigidity at the surface of silica is the predominant factor for the lack of intramolecular quenching not only by viologen but also by the 4-benzoyl-*N*-methylpyridinium cation as well. The rigidity argument is supported further by the observed photoemission—and therefore lack of quenching—from **2** in a poly(propylene sulfonate) film, namely, another room-temperature rigid environment irrelevant to silica (see Appendix S.8 in Supporting Information). In any event, the room-temperature photoluminescent behavior of the Ru(II) dyads of this study is quite reminiscent of the behavior of Ru(II) complexes entrapped in zeolites or polymeric matrixes such as cellulose acetate.[10a] Thus, again, the environmemental rigidity at the surface of silica raises the energy level of the ^{3}dd state and increases the lifetime of the emitting ^{3}MLCT state. Meanwhile, biexponential photoluminescence decay from

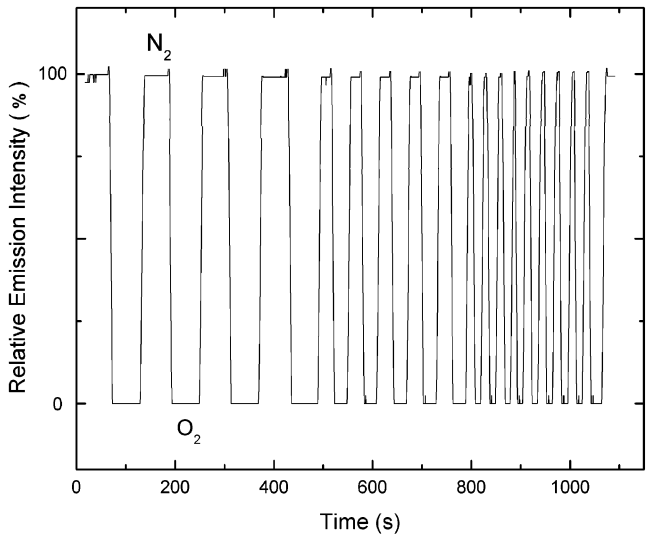

Figure 10. Room-temperature response of a silica aerogel doped with **1** under an alternating stream of N_2 and O_2. The fastest switching rate is 15 s; emission was monitored at 643 nm.

a single dopant on silica has been associated with different microenvironments (i.e., sites of different shape or polarity).[9b,d,34,35] The fact that at 77 K the amplitude of the longer lifetime of all dyads on aerogel increases and dominates the percent contribution to the total emission output can be attributed to different restrictions imposed by the different sites on the Ru−N bond lengths, and therefore the size of the entire molecule. Thus it is plausible that the ^{3}dd state of molecules found in the long-lifetime sites should be raised more in energy than the ^{3}dd states of the molecules in the short-lived sites.

A final point that needs to be addressed concerns the blue shift of the emission spectrum upon cooling doped aerogels. Since all data indicate that the microenvironment on the surface of silica is already "rigid" at room temperature, at first glance the observed blue shift cannot be explained through a fluid-to-rigid transition and the associated inhibition in the reorganization of the solvent dipoles. Similar blue shifts observed with other Ru(II) complexes entrapped in xerogels have been attributed to residual solvent remaining in the monoliths.[9c] Thermogravimetric analysis of freshly made native aerogels (Appendix S.9) shows loss of mass below 100 °C, which depends on the processing conditions: regular processing[4] results in ∼4% weight loss; additional washes with water during processing, like those employed here, results in aerogels, showing an ∼11% weight loss. Upon cooling, solvent co-adsorbed on the surface of silica loses its remaining degrees of freedom and its residual "solvating" power.

3. Conclusions—A Practical Perspective

The fact that the ^{3}MLCT states of neither **1** nor **2** are quenched on silica suggests that these molecules cannot be immobilized on silica and used for optical switching. On the other hand, sol−gel glass doped with Ru(II) tris(bidentate ligand) complexes has been the subject of numerous studies in terms of sensing oxygen by means of photoluminescence quenching.[36] In the same context, it was found here that O_2 quenches the photoluminescence of **1** more efficiently than the photoluminescence of **2** or of $[Ru(phen)_3]^{2+}$, both at room temperature and at 77 K (refer to Figure 9 and note in Appendix S.10 that the same trend is observed with **1-FB** and **2-FB**). Three-point quenching plots for **1**, **2**, and $[Ru(phen)_3]^{2+}$ (Appendix S.1), obtained by recording the steady-state emission spectra of the three complexes at room temperature under N_2, air, and O_2, are all nonlinear, consistent with the fact that the complexes emit from different microenvironments. Fitting the data according to a nonlinear model for one species emitting from two different sites yields the apparent Stern−Volmer quenching constants k_{SV-1} and k_{SV-2} (refer to Appendix S.1).[36a,b,37] The k_{SV} values for the individual complexes are not very reliable (as they are based on three-point curves); however, it is quite instructive to consider them together: thus, k_{SV-1} (concerning the short-lived sites) is in the range of 0.016−0.026 $[O_2]^{-1}$, while k_{SV-2} is in the range of 1.25−2.59 $[O_2]^{-1}$, indicating that the long-lived sites are quenched much more efficiently (>50×) than the short-lived ones. Although the reason for the differences in the quenching efficiency of O_2 in the cases of **1**, **2**, and $[Ru(phen)_3]^{2+}$ is not clear at this moment, nevertheless, it seems that oxygen can modulate the emission of aerogels doped with Ru-complex/electron acceptor dyads over a wider percentage range of light intensity. This indicates that these materials can comprise platforms for optical oxygen sensors with higher dynamic range than sol−gel-based platforms incorporating Ru(II) tris(bidentate ligand) complexes themselves. Furthermore, in contrast to frozen solutions where the emission intensity increases but the luminescent moieties are inaccessible, in frozen aerogels not only the luminescence intensity is enhanced, but also the luminescent moieties are easily accessible to outside quenchers. So, in addition to their ability to show a wider dynamic range to light intensity modulation, aerogels doped with **1** and **2** and operated at 77 K are also able to show enhanced sensitivity, and to respond very fast to changes in the concentration of O_2 in their environment. Thus, in agreement to previous reports,[4] Figure 10 shows that monolithic aerogels (∼1 cm diameter, ∼3 cm long) doped with **1** are able to respond in less than 15 s to an alternating stream of N_2 and O_2 by taking advantage of the rapid gas diffusion through the mesopores. It is noted that these results compare very favorably even with Ru-complex doped sol−gel films, whose response time to gaseous mixtures is reportedly on the order of tens of seconds.[36b] The single drawback of doped aerogels as oxygen sensors is their inherent fragility. Recently, however, we developed a method of increasing the mechanical strength of aerogels by over 2 orders of magnitude, via polymer cross-linking.[33] Currently, we are working on doping those composite materials with Ru(II) complexes and studying their properties.

4. Experimental Section

Equipment and Methods. ^{1}H and ^{13}C NMR spectra were obtained with a Varian INOVA 400 MHz NMR spectrometer and are referenced versus TMS. MALDI experiments were performed on an Applied Biosystems Voyager DE Pro reflection time-of-flight mass spectrometer. Nanospray experiments were performed on an Applied Biosystems/MDS Sciex Qstar hybrid quadrupole/time-of-flight mass spectrometer. Infrared spectra were recorded on a Nicolet Magna-IR Model 750 spectrophotometer. Elemental analyses were performed by Oneida Research Services, Inc., Whiteboro, NY. Differential pulse voltammetry was carried out with a EG&G 263A potentiostat controlled by the EG&G model 270/250 Research Electrochemistry Software 4.30. Gold disk working electrodes (1.6 mm diameter, 0.0201 cm^2) and Ag/AgCl/aqueous KCl (3 M) reference electrodes were purchased from Bioanalytical Systems, Inc. Au foil (Aldrich) was employed as a counter electrode. UV−vis spectra were recorded with an Ocean Optics, Inc., model CHEM2000 miniature fiber optic spectrophotometer. Time-resolved emission data were obtained with samples

(34) (a) Narang, U.; Wang, R.; Prasad, P. N.; Bright, F. V. *J. Phys. Chem.* **1994**, *98*, 17−22. (b) MacCraith, B. D.; McDonagh, C.; O'Keeffe, G.; McEvoy, A. K.; Butler, T.; Sheridan, F. R.; Fidelma, R. *SPIE Sol−Gel Optics III* **1994**, *2288*, 518−528.

(35) Dunn, B.; Zink, J. I. *Chem. Mater.* **1997**, *9*, 2280−2291.

(36) For example see: (a) Baker, G. A.; Wenner, B. R.; Watkins, A. N.; Bright, F. *J. Sol-Gel Sci. Technol.* **2000**, *17*, 71−82. (b) Watkins, A. N.; Wenner, B. R.; Jordan, J. D.; Xu, W.; Demas, J. N.; Bright, F. V. *Appl. Spectrosc.* **1998**, *52*, 750−754. (c) Murtagh, M. T.; Shahriari, M. R.; Krihak, M. *Chem. Mater.* **1998**, *10*, 3862−3869. (d) O'Keeffe, G.; MacCraith, B. D.; McEvoy, A. K.; McDonagh, C. M.; McGilp, J. F. *Sensors Actuators B* **1995**, *29*, 226−230.

(37) Demas, J. N.; DeGraff, B. A.; Xu, W. *Anal. Chem.* **1995**, *67*, 1377−1380.

in three freeze−pump−thaw degassed and flame-sealed ampules (made of test tubes) using a system composed of an ORIEL pulsed N_2 laser model 79111 (5 ns), an ORIEL dye laser module model 79120 adjusted at 425 nm (Oriel Dye # 79151), an ORIEL Spectrograph model 77480, an InstaSpecV image intensifier/CCD detector, and a Stanford Research Systems, Inc. four-channel delay/pulse generator model DG535. Quasi "steady-state" emission spectra were recorded with the same apparatus by setting the delay time to 700 ns and the gate width to 2000 ns. Low-temperature emission data were obtained by immersing NMR tubes containing the samples into a homemade vacuum-sealed glass Dewar filled with liquid N_2 (77 K) or dry ice/acetone (−78 °C). Time-resolved spectra of aerogels were also obtained in a vacuum degassed (room temperature, 14 h) and flame-sealed test tubes (for room-temperature experiments) or NMR tubes (for experiments at 77 K). Room-temperature experiments monitoring the response of Ru complex doped aerogel monoliths to an alternating stream of O_2/N_2 were conducted using a Perkin-Elmer LS-5 fluorescence spectrophotometer, interfaced with a PC for data acquisition. Low-temparature experiments on the effect of O_2/N_2 on photoluminescence were conducted in NMR tubes using the homemade Dewar. Excited-state lifetimes were determined either by linear fitting time-resolved emission data using Excel 2000 MS or nonlinear fitting using Microcal Origin 5.0. Molecular modeling was performed using the Spartan Version 5.0.3 for SiliconGraphics software package (Wavefunction, Inc.).

Materials. Starting materials and solvents were purchased from Aldrich or Acros and, with the exception of Et_3N, $[Ru(phen)_3]Cl_2$ were used as received. Et_3N was predried over $CaSO_4$ and then distilled either from P_2O_5 or from CaH_2 under N_2 before use. $[Ru(phen)_3]Cl_2$ was purchased and metathesized to the tetrafluoroborate salt from a 1:1 (v/v) methanol:water solution with a 10% (w/v) aqueous solution of NH_4BF_4. The precipitate was collected, recrystallized from acetone/ether, and dried under vacuum. 4-(4-Ethynylbenzoyl)pyridine[16a] and free ligand 3,8-bis(4-(4-ethynylbenzoyl)pyridine)-1,10-phenanthroline (**3**) were available from previous studies.[21] 3,8-Dibromo-1,10-phenanthroline[19a] and $Ru(phen)_2Cl_2 \cdot 2H_2O$[38] were prepared according to literature procedures. The synthesis of all new compounds is described below. For (a) the proton labels used in ^1H NMR assignments, (b) the actual ^1H NMR spectra of all complexes synthesized, and (c) the mass spectra of **2-FB** and **2**, see Appendix S.2 in the Supporting Information.

Bis(1,10-phenanthroline)mono(3,8-dibromo-1,10-phenanthroline)ruthenium(II) Di(tetrafluoroborate). $Ru(phen)_2Cl_2 \cdot 2H_2O$ (0.200 g, 0.351 mmol) was dissolved in 44 mL of 1:1 (v/v) water:methanol. Nitrogen was bubbled through the solution for 15 min, 3,8-dibromo-1,10-phenanthroline (0.593 g, 1.75 mmol) was added, and the resultant solution was refluxed for 6 h under N_2. After the solution was cooled to room temperature, NH_4BF_4 (0.210 g, 2.00 mmol) dissolved in 5 mL of water was added, and all solvents were removed under reduced pressure (rotary evaporator). The residue was dissolved in acetone and filtered and diethyl ether was added. The precipitate was collected and was added as a slurry with neutral alumina/CH_2Cl_2 into a neutral alumina/CH_2Cl_2 column. The column was eluted first with CH_2Cl_2. Then the solvent was changed first to ethanol, which eluted an orange impurity, and then to CH_3CN, which eluted the orange product. The solvent was removed under reduced pressure, and the product was reprecipitated twice from acetone/diethyl ether. Subsequently, the product was dissolved in the minimum amount of acetone/water (1:1, v:v) and was extracted with ether (five times). The aqueous layer was concentrated under reduced pressure until a precipitate was formed. Crystallization was completed in an ice bath, and the product was collected and dried under vacuum at 40 °C. Received 0.150 g (34% yield); mp > 300 °C (dec). ^1H NMR (CD_3CN, 400 MHz) δ: 8.82 (2H, d, $J_{fh} = 1.98$ Hz), 8.63 (2H, dd, $J_{ac} = 1.26$ Hz, $J_{ad} = 8.32$ Hz), 8.58 (2H, dd, $J_{a'c'} = 1.26$ Hz, $J_{a'd'} = 8.32$ Hz), 8.26 (2H, d, $J_{bb'} = 8.92$ Hz), 8.23 (2H, d, $J_{bb'} = 8.92$ Hz), 8.21 (2H, s), 8.07 (2H, dd, $J_{ca} = 1.30$ Hz, $J_{cd} = 5.26$ Hz), 8.04 (2H, d, $J_{hf} = 1.98$ Hz), 7.90 (2H, dd, $J_{a'c'} = 1.30$ Hz, $J_{c'd'} = 5.26$ Hz), 7.62 (2H, dd, $J_{ad} = 5.26$ Hz, $J_{cd} = 8.32$ Hz), 7.59 (2H, dd, $J_{a'd'} = 5.26$ Hz, $J_{c'd'} = 8.32$ Hz). ^{13}C NMR (CD_3CN, 100 MHz) δ: 155.2, 154.6, 154.1, 148.9, 148.8, 147.5, 140.0, 138.2, 138.2, 132.5, 132.2, 132.0, 129.4, 129.2, 129.1, 127.0, 126.8, 122.0. IR (KBr) ν, cm^{-1}: 3416 (br. m), 3073 (w), 1567 (w), 1428 (m), 1100 (m), 1075 (s), 1060 (s), 1025 (s), 843 (m), 722 (m). UV−vis (CH_3CN) λ_{max}, nm (ϵ, $M^{-1}\,cm^{-1}$): 203 (60 184), 223 (59 761), 234 sh (49 607), 243 (43 895), 263 (78 588), 277 sh (54 049), 433 (14 808). UV−vis (EtOH) λ_{max}, nm (ϵ, $M^{-1}\,cm^{-1}$): 220 (46 338), 234 sh (37 302), 246 sh (33 711), 263 (71 824), 277 (48 423), 319 sh (8225), 431 (13 670). Emission (CH_3CN) λ_{max}, nm, 633; τ, ns, 2216; emission (EtOH) λ_{max}, nm, 629; τ, ns, 983. Anal. Calcd for $RuC_{36}H_{22}N_6Br_2B_2F_8$: C, 44.44; H, 2.28; N, 8.64. Found: C, 44.43; H, 2.21; N, 8.50.

Bis(1,10-phenanthroline)mono(3,8-bis(4-(4-ethynylbenzoyl)pyridine)-1,10-phenanthroline)ruthenium(II) Di(tetrafluoroborate) Monohydrate (1-FB). Bis(1,10-phenanthroline)mono(3,8-dibromo-1,10-phenanthroline)ruthenium(II) di(tetrafluoroborate) (0.698 g, 0.717 mmol), $(Ph_3P)_2PdCl_2$ (0.081 g, 0.12 mmol), and CuI (0.022 g, 0.12 mmol) were combined in 60 mL of dry DMF and 15 mL of Et_3N. After the mixture was stirred for 1 h under N_2, 4-(4-ethynylbenzoyl)pyridine (0.372 g, 1.80 mmol) was added, and the color of the mixture changed quickly from red to black. The mixture was stirred at room temperature for 21 h under dry N_2. At the end of the period, the reaction mixture was filtered and diethyl ether was added to the filtrate. The crude product was introduced as a solid to a CH_2Cl_2-packed neutral alumina column and eluted with a solution containing 1% saturated aqueous KNO_3, 9% water, and 90% CH_3CN. The eluted solution was concentrated under reduced pressure, and the red product was precipitated by adding a saturated aqueous NH_4BF_4 solution and cooling. The precipitate was collected by vacuum filtration and was introduced to a second neutral alumina column packed with CH_2Cl_2. The solvent was slowly brought to 10% MeOH to elute the red product. Solvents were removed under reduced pressure, and the red product was dissolved in CH_3CN, filtered, precipitated with ether, and dried under vacuum at 40 °C. Received 0.731 g (yield 83%); mp > 300 °C (dec). ^1H NMR (CD_3CN, 400 MHz) δ: 8.79 (4H, dd, $J_{ek'} = 1.64$ Hz, $J_{ek} = 4.40$ Hz), 8.78 (2H, d, $J_{fh} = 1.64$ Hz), 8.64 (2H, dd, $J_{ac} = 1.28$ Hz, $J_{ad} = 8.33$ Hz), 8.59 (2H, dd, $J_{a'c'} = 1.28$ Hz, $J_{a'd'} = 8.33$ Hz), 8.29 (2H, s), 8.28 (2H, d, $J_{bb'} = 8.97$ Hz), 8.25 (2H, d, $J_{bb'} = 8.97$ Hz), 8.22 (2H, d, $J_{hf} = 1.64$ Hz), 8.14 (2H, dd, $J_{ca} = 1.24$ Hz, $J_{cd} = 5.26$ Hz), 7.93 (2H, dd, $J_{a'c'} = 1.24$ Hz, $J_{c'd'} = 5.26$ Hz), 7.81 (4H, d of overlapping dd (AA′, XX′), $J_m \sim J_p \sim 2-4$ Hz, $J_o = 8.24$ Hz), 7.64 (2H, dd, $J_{ad} = 5.31$ Hz, $J_{cd} = 8.24$ Hz), 7.61 (4H, d of overlapping dd (AA′, XX′), $J_m \sim J_p \sim 2-4$ Hz, $J_o = 8.24$ Hz), 7.60 (2H, dd, $J_{a'd'} = 5.31$ Hz, $J_{c'd'} = 8.24$ Hz), 7.56 (4H, dd, $J_{ke'} = 1.64$ Hz, $J_{ke} = 4.40$ Hz). ^{13}C NMR (CD_3CN, 100 MHz) δ: 195.4, 155.9, 154.5, 154.0, 151.5, 149.0, 148.9, 147.9, 144.8, 140.1, 138.1, 137.5, 132.9, 132.2, 132.1,131.8, 131.3, 129.7, 129.2, 127.2, 127.1, 126.9, 123.7, 122.8, 95.2, 88.4. IR (KBr) ν, cm^{-1}: 3409 (br s), 3053 (w), 2912 (w), 1668 (s), 1595 (s), 1430 (m), 1405 (m), 1280 (s), 1090 (s), 1064 (s), 1037 (s), 937 (m), 843 (m), 722 (m), 675 (m). UV−vis (CH_3CN) λ_{max}, nm (ϵ, $M^{-1}\,cm^{-1}$): 202 (96 393), 225 (90 278), 234 sh (68 408), 263 (97 119), 292 (64 158), 302 sh (59 391), 361 (77 322), 380 sh (64 677), 434 (16 273). UV−vis (MeOH) λ_{max}, nm (ϵ, $M^{-1}\,cm^{-1}$): 223 (90 171), 263 (97 340), 292 (64 260) 304 (57 609), 364 (69 183), 383 sh (57 437), 438 (16 410). UV−vis (EtOH) λ_{max}, nm (ϵ, $M^{-1}\,cm^{-1}$): 226 (51 140), 264 (57 360), 292 (38 563) 304 (35 314), 364 (43 607), 385 sh (34 831), 434 (10 781). For photoluminescence data, see Table 1. Anal. Calcd for $RuC_{64}H_{38}N_8O_2B_2F_8 \cdot H_2O$: C, 61.80; H, 3.24; N, 9.09. Found: C, 61.19; H, 3.15; N, 8.75.

Bis(1,10-phenanthroline)mono(3,8-bis(*N*-methyl-4-(4-ethynylbenzoyl)pyridinium)-1,10-phenanthroline)ruthenium(II) Tetra(tetrafluoroborate) Monohydrate (1). 1-FB (0.400 g, 0.326 mmol) was dissolved in 40 mL of CH_3NO_2 under N_2. A solution of trimethyloxonium tetrafluoroborate (0.101

(38) Giordano, P. J.; Bock, C. R.; Wrighton, M. S. *J. Am. Chem. Soc.* **1978**, *100*, 6960−6965.

g, 0.683 mmol) in 10 mL of CH_3NO_2 was added dropwise, and the reaction mixture was stirred at room temperature for 1 h under N_2. At the end of the period the solution was concentrated under reduced pressure and diethyl ether was added. The crude product was collected, mixed with an alumina/CH_2Cl_2 slurry, and introduced to a CH_2Cl_2-packed neutral alumina column. The column was eluted first with CH_2Cl_2 and then with a CH_2Cl_2/CH_3OH 9:1 v/v solution. As the orange band of the product began to elute, the solvent was switched to CH_3CN. Solvents were removed under reduced pressure and the orange product was recrystallized twice from CH_3CN/diethyl ether and was dried under vacuum at 40 °C. Received 0.452 g (yield: 97%); mp > 300 °C (dec). ^{1}H NMR (CD_3CN, 400 MHz) δ: 8.87 (4H, d, J_{ek} = 6.50 Hz), 8.79 (2H, d, J_{fh} = 1.65 Hz), 8.64 (2H, dd, J_{ac} = 1.28 Hz, J_{ad} = 8.24 Hz), 8.58 (2H, dd, $J_{a'c'}$ = 1.28 Hz, $J_{a'd'}$ = 8.24 Hz), 8.30 (2H, s), 8.27 (2H, d, $J_{bb'}$ = 8.97 Hz), 8.24 (2H, d, $J_{b'b}$ = 8.97 Hz), 8.22 (2H, d, J_{hf} = 1.65 Hz), 8.15 (4H, d, J_{ke} = 6.50 Hz), 8.13 (2H, dd, J_{ca} = 1.28 Hz, J_{cd} = 5.22 Hz), 7.92 (2H, dd, $J_{c'a'}$ = 1.28 Hz, $J_{c'd'}$ = 5.22 Hz), 7.81 (4H, d of overlapping dd (AA′, XX′), $J_m \sim J_p \sim 2-4$ Hz, J_o = 8.24 Hz), 7.67 (2H, dd, J_{da} = 5.31 Hz, J_{dc} = 8.24 Hz), 7.65 (4H, d of overlapping dd (AA′, XX′), $J_m \sim J_p \sim 2-4$ Hz, J_o = 8.24 Hz), 7.60 (2H, dd, $J_{a'd'}$ = 5.31 Hz, $J_{c'd'}$ = 8.24 Hz), 4.40 (6H, s). ^{13}C NMR (CD_3CN, 100 MHz) δ: 192.0, 155.9, 154.5, 154.0, 152.4, 149.0, 148.9, 148.0, 147.5, 140.3, 138.2, 138.1, 135.7, 133.2, 132.2, 132.2, 131.8, 131.6, 129.7, 129.2, 128.5, 128.3, 127.1, 126.9, 122.6, 118.4, 94.9, 89.2, 49.7. IR (KBr) ν, cm^{-1}: 3416 (br, s), 3033 (w), 2919 (w), 1669 (m), 1640 (m), 1600 (m), 1428 (m), 1290 (m), 1085 (s), 1065 (s), 1040 (s), 944 (w), 855 (w), 770 (w), 722 (w). UV−vis (CH_3CN) λ_{max}, nm (ϵ, M^{-1} cm^{-1}): 204 (102 332), 222 (94 190), 263 (110 474), 290 sh (61 620), 365 (83 333), 385 sh (66 345), 437 (16 586). UV−vis (MeOH) λ_{max}, nm (ϵ, M^{-1} cm^{-1}): 222 (83 557), 263 (111 354), 298 sh (56 088), 365 (70 069), 383 sh (57 240), 437 (16 284). UV−vis (EtOH) λ_{max}, nm (due to low solubility, ϵ values are not reported): 221, 263, 290 (sh), 302 (sh), 366, 386 (sh). For photoluminescence data, see Table 1. Anal. Calcd for $RuC_{66}H_{44}N_8O_2B_4F_{16}\cdot H_2O$: C, 54.77; H, 3.20; N, 7.74. Found: C, 54.25; H, 3.02; N, 7.70.

4-(1,2-Dibromoethyl)toluene. Bromine (110 mL, 2.15 mol) was added dropwise under nitrogen to 4-methylstyrene (224 g, 1.90 mol) in 1 L of $CHCl_3$ at 0 °C. The resultant solution was allowed to reach room temperature and was washed consecutively with a saturated aqueous sodium bisulfite solution, water, and a saturated NaCl solution. The organic layer was dried over $MgSO_4$. The solvent was removed under reduced pressure and the resultant colorless oil crystallized slowly upon cooling in the refrigerator. The product was dried under vacuum. Received 493 g (yield 94%); mp 39−41 °C. ^{1}H NMR ($CDCl_3$, 400 MHz) δ: 7.28 (2H, dt, J = 2.02 Hz, J = 3.76 Hz, J = 8.34 Hz), 7.17 (2H, d, J = 7.87 Hz), 5.13 (1H, q, J = 5.50 Hz, J = 10.63 Hz), 4.03 (2H, m), 2.33 (3H, s). ^{13}C NMR ($CDCl_3$, 100 MHz) δ: 139.18, 135.62, 129.54, 127.48, 51.02, 35.04, 21.25. IR (KBr, cm^{-1}): 3050 (w), 2930 (w), 2860 (w), 1505 (m), 1440 (m), 1425 (m), 1150 (m), 820 (s), 715 (s), 595 (s). GC-MS *m*/*z* (rel intensity): 197 (33), 117 (100), 91 (26).

4-Ethynyltoluene. 4-(1,2-Dibromoethyl)toluene (215 g, 0.77 mol) was added under nitrogen to a refluxing solution of potassium *tert*-butoxide (181 g, 1.6 mol) in 3.5 L of *tert*-butyl alcohol. Reflux was continued for 1 h; then the solution was allowed to cool to room temperature and was poured into 10.5 L of an ice/water mixture. The solution was saturated with NaCl and was extracted with diethyl ether three times. The combined extracts were dried over $MgSO_4$. Solvents were removed under reduced pressure and the colorless oil was dried further under vacuum at room temperature. Received 44 g (49% yield). ^{1}H NMR ($CDCl_3$, 400 MHz) δ: 7.37 (2H, dt, J = 1.74 Hz, J = 3.58 Hz, J = 8.14 Hz), 7.10 (2H, dm), 3.01 (1H, s), 2.33 (3H, s). ^{13}C NMR ($CDCl_3$, 100 MHz) δ: 138.89, 131.97, 129.02, 119.01, 83.80, 76.44, 21.42. IR (KBr), ν, cm^{-1}: 3298 (s), 3070 (w), 3035 (m), 2910 (m), 2880 (w), 2100 (m), 1510 (s), 815 (s), 655 (s), 640 (s), 608 (s), 530 (s). GC-MS *m*/*z* (rel intensity): 116 (M, 78), 115 (100), 89 (10), 63 (27), 39 (26).

4-(Trimethylsilylethynyl)toluene. A solution (2.5 M) of butyllithium in hexane (145 mL, 362 mmol) was added dropwise to a solution of 4-ethynyltoluene (40 g, 344 mmol) in 600 mL of diethyl ether at −78 °C. The mixture was stirred for 1 h under N_2, chlorotrimethylsilane (53 mL, 0.42 mol) was added slowly, and the solution was allowed to warm to room temperature. The contents of the flask were added into 630 mL of a saturated aqueous NH_4Cl solution and the layers were separated. The aqueous layer was extracted (3×) with 200 mL of ether. The combined organic layers were dried over $MgSO_4$, filtered, and concentrated under reduced pressure. The crude product was distilled under vacuum to a clear liquid that solidifies to a white solid right above room temperature. Received 58 g (89% yield); mp 32−34 °C. ^{1}H NMR ($CDCl_3$, 400 MHz) δ: 7.35 (2H, dt, J = 1.83 Hz, J = 3.48 Hz, J = 8.24 Hz), 7.08 (2H, dd, J = 0.55 Hz, J = 8.43 Hz), 2.33 (3H, s), 0.25 (9H, s). ^{13}C NMR ($CDCl_3$, 100 MHz) δ: 138.53, 131.80, 128.88, 120.02, 105.32, 93.15, 21.43, −0.03. IR (KBr) ν, cm^{-1}: 3030 (w), 2960 (s), 2905 (w), 2890 (w), 2155 (s), 1510 (s), 1250 (s), 870 (s), 845 (s), 810 (s), 765 (s), 538 (s). GC-MS *m*/*z* (rel intensity): 188 (M, 25), 173 (100).

1-Bromomethyl-4-(trimethylsilylethynyl)benzene. 4-(Trimethylsilylethynyl)toluene (25 g, 133 mmol), *N*-bromosuccinimide (25 g, 139 mmol, recrystallized from water), benzoyl peroxide (0.379 g, 1.56 mmol), and 300 mL of dry CCl_4 (predried over $CaCl_2$ and distilled under N_2 from P_2O_5) were combined and refluxed under N_2 for 23 h. The mixture was then cooled in an ice bath and filtered. CCl_4 was removed under reduced pressure and the resultant oil was introduced to a silica gel column with hexane. Unreacted 4-(trimethylsilylethynyl)toluene was eluted with hexane and the desired product with a 1:1 (v/v) hexane:$CHCl_3$ mixture. Solvents were removed under reduced pressure and the product was obtained as a light yellow liquid. Received 10 g (28% yield). ^{1}H NMR ($CDCl_3$, 400 MHz) δ: 7.41 (2H, dd, J = 1.83 Hz, J = 6.59 Hz), 7.29 (2H, dd, J = 1.74 Hz, J = 6.50 Hz), 4.43 (2H, s), 0.25 (9H, s). ^{13}C NMR ($CDCl_3$, 100 MHz) δ: 137.94, 132.25, 128.86, 123.22, 104.44, 95.18, 32.83, −0.095. IR (KBr) ν, cm^{-1}: 3055 (w), 2960 (s), 2900 (w), 2160 (s), 1505 (s), 1410 (m), 1250 (s), 1220 (s), 870 (s), 840 (s), 765 (s), 640 (s), 605 (s). GC-MS *m*/*z* (rel intensity): 267 (M, 8), 252 (18), 187 (100), 172 (28), 86 (11).

1-Bromomethyl-4-ethynylbenzene. KF (6.529 g, 112.4 mmol) in 20 mL of H_2O was added to a solution of 1-bromomethyl-4-(trimethylsilylethynyl)benzene (10 g, 37.5 mmol) in 120 mL of 1:1 (v/v) CH_3OH/THF, and the mixture was stirred for 18 h under N_2, at room temperature. Subsequently, the mixture was poured into 150 mL of H_2O and extracted three times with 100 mL portions of diethyl ether. The combined extracts were dried over $MgSO_4$, all solvents were removed under reduced pressure, and the orange oil was passed through a silica column eluting with a 7:3 (v/v) hexane/CH_2Cl_2 solution. Solvents were removed under reduced pressure and the yellow solid was dried under vacuum. Received 6.22 g (85% yield); mp 35−38 °C. ^{1}H NMR ($CDCl_3$, 400 MHz) δ: 7.46 (2H, d, J = 8.24 Hz), 7.35 (2H, d, 8.25 Hz), 4.48 (2H, s), 3.10 (1H, s). ^{13}C NMR ($CDCl_3$, 100 MHz) δ: 138.37, 132.49, 128.99, 122.22, 83.08, 78.06, 32.73. IR (KBr, cm^{-1}): 3275 (s), 1500 (m), 1400 (m), 1220 (s), 1206 (m), 840 (s), 825 (m), 680 (s), 625 (m), 600 (s). GC-MS *m*/*z* (rel intensity): 195 (M, 20), 115 (100).

***N*-(4-Ethynylbenzyl)-4,4′-bipyridinium Tetrafluoroborate.** (The synthesis of this key intermediate and its precursors is summarized in Appendix S.3 of the Supporting Information.) 1-Bromomethyl-4-ethynyl-benzene (0.392 g, 2.01 mmol) was dissolved in 20 mL of anhydrous benzene and the solution was added dropwise under N_2 to 4,4′-bipyridine (1.22 g, 7.83 mmol, recrystallized from benzene/hexane) dissolved in 20 mL of anhydrous benzene. The reaction mixture was refluxed for 6 h, and the total volume was reduced to 20 mL. The yellow solid was collected, washed with ether (received 0.45 g), and redissolved in water. Precipitation was induced by adding an aqueous NH_4BF_4 solution (2 g in 20 mL). NMR analysis showed that at this point the main byproduct was the diquaternized salt. Purification was carried out by adding the crude product in 300 mL of boiling CH_2Cl_2 and by filtering the mixture quickly while hot. CH_2Cl_2 was removed under reduced pressure, the precipitate was dissolved in hot water,

and the solution was treated with activated carbon, filtered, and cooled to induce crystallization of a white solid. Received 0.3 g (42% yield); mp 82.5−83.5 °C. ^{1}H NMR (400 MHz, CD_3CN) δ: 8.83 (2H, dd, J = 1.6 Hz, J = 4.4 Hz), 8.81 (2H, d, J = 7.2 Hz), 8.3 (2H, d, J = 7.2 Hz), 7.76 (2H, dd, J = 4.4 Hz, J = 1.6 Hz), 7.58 (2H, d, J = 8.3 Hz), 7.46 (2H, d, J = 8.4 Hz), 5.75 (2H, s), 3.50 (1H, s). ^{13}C NMR (100 MHz, CD_3CN) δ: 155.63, 152.1, 146.01, 142.08, 134.54, 133.85, 133.86, 130.37, 130.35, 127.26, 124.54, 122.85, 122.79, 80.62, 80.49, 64.52. IR (KBr pellet) ν: 3409 (br s), 3241 (m), 3181 (m), 3120 (m), 3040 (m), 2106 (w), 1636 (s), 1602 (m), 1542 (m), 1461 (m), 1428 (m), 1166 (m), 1038 (br s), 823 (s), 769 (m), 722 (m), 696 (w). MALDI mass spectrometric analysis: mass formula $(C_{19}H_{15}N_2)^+$. Theoretical mass: 271.1230 *m*/*z*. Found: 271.1260 *m*/*z*.

Bis(1,10-phenanthroline)mono(3,8-bis(*N*-(4-ethynylbenzyl)-4,4′-bipyridinium)-1,10-phenanthroline)ruthenium(II) Tetra(tetrafluoroborate) (2-FB). Bis(1,10-phenanthroline)mono(3,8-dibromo-1,10-phenanthroline)ruthenium(II) ditetrafluoroborate (0.3 g, 0.308 mmol), Et_3N (7 mL), $(Ph_3P)_2PdCl_2$ (0.035 g, 0.050 mmol), CuI (0.011 g, 0.059 mmol), and anhydrous DMF (10 mL) were combined in a flame-dried flask under N_2. The mixture was stirred under N_2 for 40 min. At the end of the period, a N_2-degassed solution of *N*-(4-ethynylbenzyl)-4,4′-bipyridinium tetrafluoroborate (0.273 g, 0.763 mmol) in 10 mL of DMF was transferred into the reaction mixture through a needle. The reaction mixture turned from red to black and was stirred for 24 h. At the end of the period, NH_4BF_4 (0.977 g, 9.322 mmol) was added to the reaction all at once and the mixture was stirred for another 30 min. Subsequently, the mixture was filtered and diethyl ether was added to the filtrate until no more precipitation was observed. The red solid was collected, treated with CH_3CN, and filtered again and the filtrate was evaporated to dryness. The solid was treated with THF and filtered and the red crystals were collected. The crude product (0.49 g) was dissolved in CH_3CN and was purified by column chromatography (silica packed with CH_3CN and eluted first with CH_3CN and then with a solution containing 5% water saturated with $NaNO_3$, 25% H_2O, and 70% CH_3CN). A large amount of NH_4BF_4 was added to the eluted solution, and upon removal of the CH_3CN with the rotary evaporator, the product precipitated in the remaining aqueous solution. The solid was collected, dried in a vacuum, redissolved in CH_3CN, and precipitated with diethyl ether. Received 0.35 g of the orange product (yield 78%); mp > 195 °C (dec). ^{1}H NMR (400 MHz, CD_3CN) δ: 8.89 (4H, dd, J_{ke}= 2.02 Hz, $J_{ke'}$ = 7.15 Hz), 8.83 (4H, dd, J_{ek} = 1.84 Hz, $J_{ek'}$= 4.4 Hz), 8.71 (2H, d, J_{fh}= 1.64 Hz), 8.62 (2H, dd, J_{ac} = 1.28 Hz, J_{ad} = 8.24 Hz), 8.56 (2H, dd, $J_{a'c'}$ = 1.28 Hz, $J_{a'd'}$ = 8.42 Hz), 8.32 (4H, dd, J_{lm} = 1.47 Hz, $J_{lm'}$ = 7.15 Hz), 8.26 (2H, s), 8.26 (2H, d, $J_{bb'}$ = 8.97 Hz), 8.24 (2H, d, $J_{b'b}$ = 8.97 Hz), 8.15 (2H, d, J_{hf} = 1.65 Hz), 8.1 (2H, dd, J_{ca} = 1.28 Hz, J_{cd} = 5.13 Hz), 7.91 (2H, dd, $J_{c'a'}$ = 1.29 Hz, $J_{c'd'}$ = 5.13 Hz), 7.77 (4H, dd, J_{ml} = 1.64 Hz, $J_{ml'}$= 4.39 Hz), 7.66 (2H, dd, J_{da} = 5.12 Hz, J_{dc} = 8.24 Hz), 7.58 (2H, dd, $J_{d'a'}$ = 5.31 Hz, $J_{d'c'}$ = 8.24 Hz), 7.51 (8H, dd, J_{ij} = 8.61 Hz, J_{ji}= 15.57 Hz), 5.77(4H, s). ^{13}C NMR (CD_3CN, 100 MHz) δ: 155.71, 155.59, 154.40, 153.94, 152.18, 148.89, 148.78, 147.69, 146.22, 142.06, 139.86, 138.06, 138.02, 135.64, 133.48, 132.099, 132.038, 131.67, 130.66, 130.48, 129.54, 129.07, 127.29, 127.20, 126.96, 126.81, 123.76, 122.86, 122.81, 95.26, 86.59, 64.15. IR (KBr) ν, cm^{-1}: 3416 (br s), 3120 (m), 3046 (m), 2925 (sh), 2220 (w), 1629 (m), 1596 (w), 1381 (s), 1085 (w), 857 (w), 823 (w), 722 (w). UV−vis (CH_3CN) λ_{max}, nm (ϵ, M^{-1} cm^{-1}): 202 (101 410), 222 (80 695), 263 (122 280), 293 sh (66 937), 336 sh (44 212), 360 (58 280), 446 (13 758). UV−vis (CH_3OH) λ_{max}, nm (ϵ, M^{-1} cm^{-1}): 212 (82 313), 224 (78 011), 263 (121 892), 301 sh (44 497), 338 sh (43 594), 361-(56 931), 457 (10 755). For photoluminescence data see Table 1. Anal. Calcd for $RuC_{74}H_{50}N_{10}B_4F_{16}\cdot 3H_2O$: C, 56.19; H, 3.57; N, 8.85. Found: C, 56.68; H, 3.68; N, 8.34. Nanospray mass spectrometric analysis (see Appendix S.1 in Supporting Information): Formula, $(C_{74}H_{50}N_{10}RuB_3F_{12})^+$; theoretical mass, 1441.3390 *m*/*z*; found, 1441.3431 *m*/*z*. Formula, $(C_{74}H_{50}N_{10}RuB_2F_8)^{2+}$; theoretical mass, 677.1674 *m*/*z*; found, 677.1370 *m*/*z*. Formula, $(C_{74}H_{50}N_{10}RuBF_4)^{3+}$; theoretical mass, 422.4435 *m*/*z*; found, 422.4203 *m*/*z*.

Bis(1,10-phenanthroline)mono[3,8-bis(*N*-(4-ethynylbenzyl)-*N*-methyl-4,4′-bipyridinium)-1,10-phenanthroline)]ruthenium(II) Hexa(tetrafluoroborate) (2). 2-FB (0.2 g, 0.131 mmol) was dissolved in 20 mL of CH_3NO_2 under N_2. Trimethyloxonium tetrafluoroborate (0.155 g, 1.046 mmol) in 10 mL of CH_3NO_2 was added dropwise and the resulting solution was stirred under N_2 for 6 h. At the end of the period, MeOH (2 mL) was added to quench the excess of trimethyloxonium tetrafluoroborate, the solution was concentrated under reduced pressure, and the product was precipitated with diethyl ether. The product was redissolved in CH_3CN and reprecipitated with diethyl ether. Received 0.21 g of the red product (92% yield), mp > 220 °C (dec). ^{1}H NMR (400 MHz, CD_3CN) δ: 8.94 (4H, dd, J_{ke} = 1.83 Hz, $J_{ke'}$ = 7.14 Hz), 8.85 (4H, J_{ek} = 6.78 Hz), 8.72 (2H, d, J_{fh} = 1.65 Hz), 8.62 (2H, dd, J_{ac} = 1.28 Hz, J_{ad} = 8.24 Hz), 8.56 (2H, dd, $J_{a'c'}$ = 1.28 Hz, $J_{a'd'}$ = 8.42 Hz), 8.42 (4H, dd, J_{lm} = 2.01 Hz, $J_{lm'}$ = 7.14 Hz), 8.37 (4H, d, J_{ml} = 6.78 Hz), 8.27 (2H, s), 8.26 (2H, d, $J_{bb'}$ = 8.98 Hz), 8.24 (2H, d, $J_{b'b}$ = 8.97 Hz), 8.16 (2H, d, J_{hf} = 1.65 Hz), 8.12 (2H, dd, J_{ca} = 1.28 Hz, J_{cd} = 5.13 Hz), 7.91 (2H, dd, $J_{c'a'}$ = 1.29 Hz, $J_{c'd'}$ = 5.13 Hz), 7.66 (2H, dd, J_{da} = 5.12 Hz, J_{dc} = 8.24 Hz), 7.59 (2H, dd, $J_{d'a'}$ = 5.31 Hz, $J_{d'c'}$ = 8.24 Hz), 7.52 (8H, dd, J_{ij} = 8.61 Hz, J_{ji} = 19.41 Hz), 5.81 (4H, s), 4.39 (6H, s). ^{13}C NMR (CD_3CN, 100 MHz) δ: 155.70, 154.38, 153.92, 151.46, 150.41, 148.84, 148.73, 147.66, 147.47, 146.67, 143.80, 138.86, 138.03, 137.98, 134.95, 133.53, 132.05, 132.01, 131.64, 130.76, 129.52, 129.04, 128.59, 128.42, 127.81, 127.70, 126.95, 126.80, 123.94, 122.79, 95.11, 86.71, 64.96, 49.53. IR (KBr) ν, cm^{-1}: 3402 (br s), 3113 (w), 3033 (m), 2925 (sh w), 2872 (sh w), 2213 (w), 1763 (w), 1643 (m), 1508 (w), 1421 (m), 1045 (br s), 850 (w), 823 (w), 790 (w), 521 (w). UV−vis (CH_3CN) λ_{max}, nm (ϵ, M^{-1} cm^{-1}): 203 (88 734), 224 (70 956), 262 (114 086), 293 sh (63 381), 360 (58 280), 446 (13 758). UV−vis (CH_3OH) λ_{max}, nm (ϵ, M^{-1} cm^{-1}): 213 (74 713), 222 (73 852), 263 (116 156), 300 sh (50 497), 337 sh (43 164), 362 (58 795), 459 (10 325). For photoluminescence data, see Table 1. Nanospray mass spectrometric analysis (see Appendix S.1 in Supporting Information): Formula, $(C_{76}H_{56}N_{10}RuB_5F_{20})^+$; theoretical mass, 1645.3924 *m*/*z*; found, 1645.4371 *m*/*z*. Formula, $(C_{76}H_{56}N_{10}RuB_4F_{16})^{2+}$; theoretical mass, 779.1944 *m*/*z*; found, 779.1843 *m*/*z*. Formula, $(C_{76}H_{56}N_{10}RuB_2F_8)^{4+}$; theoretical mass, 364.0950 *m*/*z*; found, 364.0770 *m*/*z*.

Preparation and Doping of Silica Hydrogels and Aerogels. Silica hydrogels were prepared according to a single-step base-catalyzed route by mixing two solutions, one (solution A) containing 3.839 mL of tetramethoxysilane (TMOS, Alfa/Aesar) and 4.5139 mL of methanol (Mallinckrodt) and another (solution B) containing 4.5139 mL of methanol, 1.5139 mL of 18 MΩ-cm water (DIUF, deionized ultrafiltered), and 20 μL of NH_4OH (30% in water, Aldrich).[4] Solution B was added to solution A with stirring, and the resulting solution was poured into 1 cm in diameter polyethylene vials, covered with Parafilm to prevent solvent evaporation, and left to gel (∼15 min) and subsequently to age (48 h). At the end of the aging period, all gels were removed from their molds and placed in 20-mL vials filled with methanol. Methanol was changed five times, once every 2 h. Subsequently, methanol was replaced with HPLC water, which was changed four times over a period of 2 days. Finally, water was replaced by methanol again, which was changed another three times over a period of a day. At this point, silica hydrogels were doped with Ru(II) complexes by placing them in methanolic solutions (20 mL) of the desired complexes (∼1×10^{-5} M). Within a few hours, the baths were decolorized completely, and the orange or red gels (depending on the complex) were removed and washed with methanol three times over a period of 1 day. No leaching of the complexes from the gels was observed. Finally, samples were soaked in acetone overnight, followed by washing in acetone (five times, once every 2 h). After a second overnight residence in acetone, the samples were transferred fully submerged in acetone into a cooled (10−13 °C) autoclave (SPI Supplies, West Chester, PA), and acetone was extracted with liquid CO_2 over a period of 3−4 h. Subsequently, the pore liquid was taken supercritically by increasing the temperature and pressure inside the autoclave above the critical point of

CO_2 (31 °C, 7.4 MPa). The transition over the critical point is confirmed by the disappearance of the meniscus at the surface of the liquid CO_2. The samples were kept under supercritical CO_2 for ~30 min to ensure thermal equilibrium in the micropores, and subsequently gaseous CO_2 was vented off slowly over 45 min.

Acknowledgment. We gratefully acknowledge support by the NASA Glenn Research Center Director's Discretionary Fund (DDF), by the Vehicle Systems Program, and by the Petroleum Research Fund, administered by the ACS (Grant No. 35154-AC).

Supporting Information Available: Appendix S.1, Stern Volmer plots; Appendix S.2, proton assignment for NMR, ^1H NMRs, and representative mass spectra; Appendix S.3, synthesis of *N*-(4-ethynylbenzyl)-4,4′-bipyridinium tetrafluoroborate; Appendix S.4, electronic absorption data in the MLCT region for all Ru(II) complexes; Appendix S.5, results from MO calculations; Appendix S.6, example of bioexponential emission decay data and fitting; Appendix S.7, comparison of emission data from doped aerogels at 77 K and from frozen methanol; Appendix S.8, emission data from **2** in a poly(propylene sulfonate); Appendix S.9, thermogravimetric analysis (TGA) data for native silica aerogels; Appendix S.10, emission spectra at 77 K of aerogels doped with **1-FB** or **2-FB** under O_2 and N_2. This material is available free of charge via the Internet at http://pubs.acs.org.

CM034999B